

Gravitational Lensing of Euler-Heisenberg Black Hole Surrounded by Perfect Fluid Dark Matter

Ping Su ^{*}and Chen-Kai Qiao [†]

College of Science, Chongqing University of Technology, Banan, Chongqing, 400054, China

February 11, 2025

Abstract

In this work, we study the gravitating lensing Euler-Heisenberg black hole surrounded by perfect fluid dark matter. This kind of black hole solution enables us to investigate the nontrivial interplay between the dark matter effects and nonlinear electrodynamics effects (or quantum electrodynamics effects) on charged black hole systems. The important observables in gravitational lensings are calculated and discussed in our work, including the gravitational deflection angle of light, time delay of light, precession angle of massive orbit's bound orbits, and black hole shadow radius. The results indicates that the Euler-Heisenberg black hole with a larger perfect fluid dark matter parameter could greatly reduce the gravitational deflection angle of light, time delay of light and precession angle of massive object's bound orbit, while the nonlinear electrodynamics effects do not have large influences on these gravitational lensing observables.

Keywords: Euler Heisenberg Black Hole; Gravitational Lensing;
Perfect Fluid Dark Matter; Nonlinear Electrodynamics Effects

1 Introduction

In the past few decades, modern astrophysical observations reveal that most of our universe is dominated by dark matter and dark energy. Particularly, the cosmic microwave background (CMB) observations suggested that 26.8% of our universe is consist of dark patter, 68.3% of our universe is composed of dark energy, while only 4.9% of our universe is composed of baryonic matter [1–4]. Theoretically, the unknown dark matter are composed of unknown particles predicted in theories beyond the Standard Model, such as axions, sterile neutrinos and weakly interactive massive particles(WIMPs). In astronomy, the dark matter have extremely strong influences on the structure and formation of galaxy clusters, and it can also dominantly affects the star motions in galaxies and galaxy clusters, producing observational flat rotational curves in spiral galaxies [5–8]. Notably, recent studies also suggested that galactic dark matter halo have non-negligible influences on the gravitational lensing and shadow images of supermassive black holes [9–26].

The equation of state for dark matter in galaxies (around the supermassive black hole in the galaxy center) is still a mystery. Recently, a perfect fluid dark matter (PFDM) model has attracted large interests [27–29]. Despite the simple form of PFDM model, it can reflect some non-trial effects and characters for dark matter. In recent years, a number of studies investigate the PFDM effects on many aspects of black hole physics, and effective spacetime metrics for several kinds of black holes (such as Schwarzschild, RN, Kerr black holes) surrounded by PFDM have been successfully constructed [30–34]. Based on these effective spacetime metrics, the gravitational lensing, black hole shadow images, quasi-normal mode, thermodynamic properties of black hole system in PFDM medium can be extensively analyzed [35–51].

Inspired by the simplicity and success of PFDM model in black hole physics and astronomy, we choose a novel black hole solution in PFDM medium — the Euler-Heisenberg black hole surrounded by PFDM. The Euler-Heisenberg black hole, which is obtained from the Euler-Heisenberg effective action [52–55], stimulated

^{*}Email: suping@cqut.edu.cn

[†]Email: chenkaiqiao@cqut.edu.cn

numerous studies in past few years, for its nontrivial realization on the coupling between nonlinear electrodynamics and gravity systems, especially with the quantum loop-corrections in quantum electrodynamics (QED) [56]. With these desired properties, this kind of black hole is often used to explore the nonlinear electrodynamics in black hole physics, evoking a number of studies on thermodynamic transitions, thermodynamic topology, black hole shadow, gravitational lensing, quasi-normal modes for black hole systems with nonlinear electrodynamics in recent years [57–90]. The nonlinear electrodynamics effects (or QED effects) on gravitation are extremely important issues in high energy scale, and they may have potential influences on the evolution of our universe (especially at the beginning stage), such as the inflationary theory in Big Bang, the dynamic evolution of dark matter and dark energy, and the cosmological accelerating expansion of universe. Therefore, it is interesting to study the interplay between dark matter and nonlinear electrodynamics in gravitational systems. The Euler-Heisenberg black hole surrounded by PFDM could provide us a simply way to investigate their influences on charged black holes. Recently, several analytical solution for Euler-Heisenberg black hole in the presence of dark matter medium have been constructed [91–94], which enable us to give a comprehensive exploration on the interplay dark matter effects and nonlinear electrodynamics effects in black hole systems.

In this work, we carry out an investigation on the gravitational lensing of Euler-Heisenberg black hole surrounded by PFDM. The gravitational lensing observables provide an avenue to reveal the features of gravitational field and intrinsic properties of black holes through high precision observational data [95, 96]. An exploration of gravitational lensing observables for Euler-Heisenberg black hole surround by PFDM could enrich our knowledge on the gravitational field for charged black hole systems, especially with the influences coming from the dark matter effects and nonlinear electrodynamics effects (or QED effects). Concretely, in the present work, we calculate the gravitational deflection angle of light, time delay of light, precession angle of massive object’s bound orbits for Euler-Heisenberg black hole surrounded by PFDM. There are significantly important observables in the gravitational lensing observations, which have been frequently used to test various aspects of black hole physics and gravitational theories in both strong gravitational field limit and weak gravitational field limit. Furthermore, stimulated by the rapid development of black hole shadow researches since the capture of black hole images by Event Horizon Telescope (EHT) [97–99], the black hole critical shadow radius for Euler-Heisenberg black hole in the presence of PFDM is also discussed in our work.

This rest of the present work is organized in the following way. Section 2 briefly introduces the spacetime metric generated by Euler-Heisenberg black hole surrounded by PFDM. In section 3, the theoretical approach employed in calculating the gravitational lensing observables is described in details. In section 4, numerical results and discussions on the gravitational lensing observables (gravitational deflection angle of light, time delay of light, trajectory and precession angle of massive object’s bound orbit, black hole shadow critical radius) for Euler-Heisenberg black holes surrounded by PFDM are presented. Summary and perspectives are given in section 5. Throughout this work, the natural unit $G = c = 1$ is adopted.

2 Euler-Heisenberg Black Hole Surrounded by Perfect Fluid Dark Matter

The Euler-Heisenberg black hole becomes attractive in recent year for its ability to include the nonlinear electrodynamics effects (or QED effects). This kind of black hole solution can be solved from the gravitational field equation and the Euler-Heisenberg effective action [52], and it is one of the most important realization on the coupling between nonlinear electrodynamics and charged black hole systems.

Recently, several analytical solution for Euler-Heisenberg black hole in the presence of dark matter medium have been constructed [91–94]. Particularly, S.-J. Ma *et al.* derived the effective spacetime metric for an Euler-Heisenberg black hole surrounded by PFDM, through solving the gravitational field equation coupled with nonlinear electromagnetic field (with QED effects included) and dark matter field (assumed to be PFDM) [91]. The Lagrangian of a gravitational system coupled with nonlinear electromagnetic field and dark matter field can be written as [91, 93]

$$S = \frac{1}{4\pi} \int \sqrt{-g} d^4x \cdot \left[\frac{R}{4} + \mathcal{L}_{\text{EM}} + \mathcal{L}_{\text{PFDM}} \right] \quad (1)$$

and the nonlinear electromagnetic field’s Lagrangian density is given by

$$\mathcal{L}_{\text{EM}} = -F + \frac{a}{2} F^2 + \frac{7a}{8} G^2 \quad (2)$$

where $F = \frac{1}{4}F_{\mu\nu}F^{\mu\nu}$ is electromagnetic strength tensor and $G = \frac{1}{4}F_{\mu\nu} * F^{\mu\nu}$ (the $*F_{\mu\nu}$ is the dual form of the electromagnetic strength tensor $F_{\mu\nu}$). The above Lagrangian leads to the gravitational field equation

$$R_{\mu\nu} - \frac{1}{2}Rg_{\mu\nu} = 8\pi T_{\mu\nu} \quad (3)$$

with the energy-momentum tensor contributed from nonlinear electromagnetic field and dark matter field. To derive a spherically symmetric analytical solution for black hole, the energy-momentum tensors for PFDM and nonlinear electromagnetic field are restricted to the following explicit form in the spherical coordinate [91]

$$\begin{aligned} T_{\nu}^{\mu} &= (T_t^t, T_r^r, T_{\theta}^{\theta}, T_{\phi}^{\phi}) \\ &= \frac{1}{4\pi} \left(-\frac{Q^2}{2r^4} + \frac{aQ^4}{8r^8}, -\frac{Q^2}{2r^4} + \frac{aQ^4}{8r^8}, \frac{Q^2}{2r^4} - \frac{3aQ^4}{8r^8}, -\frac{Q^2}{2r^4} + \frac{aQ^4}{8r^8} \right) \text{ Electromagnetic Field} \\ &= \left(\frac{\lambda_{\text{DM}}}{8\pi r^3}, \frac{\lambda_{\text{DM}}}{8\pi r^3}, -\frac{\lambda_{\text{DM}}}{16\pi r^3}, -\frac{\lambda_{\text{DM}}}{16\pi r^3} \right) \text{ Dark Matter Field} \end{aligned} \quad (4)$$

where M is the black hole mass, Q is the black hole electric charge, a is a parameter which measures the strength of nonlinear electrodynamics effects (or QED effects). The parameter λ_{DM} denotes the influences of PFDM, which is proportional to the dark matter density. Eventually, by solving the gravitational field equation in the spherical coordinates, the spacetime metric for an Euler-Heisenberg black hole surrounded by PFDM is

$$ds^2 = -f(r)dt^2 + \frac{1}{f(r)}dr^2 + r^2(d\theta^2 + \sin^2\theta d\phi^2) \quad (5)$$

with the metric component function $f(r)$ defined as [91]

$$f(r) = 1 - \frac{2M}{r} + \frac{Q^2}{r^2} - \frac{aQ^4}{20r^6} + \frac{\lambda_{\text{DM}}}{r} \cdot \ln \frac{r}{|\lambda_{\text{DM}}|} \quad (6)$$

In the absence of dark matter (namely $\lambda_{\text{DM}} = 0$), this metric represents an Euler-Heisenberg black hole with nonlinear electrodynamics effects. On the other hand, when $a = 0$, the nonlinear electrodynamics effects vanish and the spacetime gives a charged Reissner-Nordström (RN) black hole surrounded by PFDM. In the cases of $\lambda_{\text{DM}} = 0$ and $a = 0$, the spacetime recovers to a simple RN black hole spacetime.

In the presence of PFDM and nonlinear electrodynamics effects, the horizon of charged black hole can be greatly influenced. It is commonly known that the classical charged black hole spacetime (such as RN spacetime) could produce naked singularities when electric charge exceeds its maximal allowed value. However, the Euler-Heisenberg black hole with a nonzero nonlinear electrodynamics parameter $a > 0$ and a non-vanishing PFDM parameter $\lambda_{\text{DM}} \neq 0$ would no longer produce naked singularities for arbitrary black hole electric charge (see Appendix A). Therefore, in the rest of this work, it is safely to change black hole parameters in the calculation of gravitational lensing observables for Euler-Heisenberg black hole surrounded by PFDM, without worrying about the annoying naked singularities. The horizons of Euler-Heisenberg black hole surrounded by PFDM are discussed in the Appendix A.

As an theoretical investigation, we only consider the dark matter field and nonlinear electromagnetic field in this work. The influences from other complex matter fields (such as disk structure in galaxies composed of luminous stars, dusts and plasma in galaxies) are not included in our work. Since the energy-momentum tensor of the dark matter fluid is spherically symmetric, they can form a spherically symmetric halo structure around the central supermassive black hole. In this work, we assume that the event horizon of Euler-Heisenberg black hole (surrounded by PFDM) r_H , the scale of dark matter halo r_{halo} , and the impact parameter for particle orbits b satisfy

$$r_H \ll b \ll r_{\text{halo}} \quad (7)$$

Furthermore, it should be mentioned that the PFDM model which gives rise to the black hole solution in (6) is a very simplified perfect fluid model. In such simplified model, the energy-momentum tensor of PFDM contains only one free parameter λ_{DM} , so the energy density ρ and pressure P of the isotropic dark matter fluid are directly linked with λ_{DM} via expression (4). The spacetime metric of black holes in this simple dark matter model satisfies $g_{tt} \times g_{rr} = -1$. Recently, some studies have explored more complex perfect fluid models for dark matter. In these dark matter fluid models, the energy-momentum tensor of dark matter fluid contains the energy density ρ and the pressures in radial direction and tangential direction (parameterized by P_r and P_t), and they are connected through the equation of state for dark matter fluids [100–103]. Especially,

some researchers are interested in the Tolman-Oppenheimer-Volkoff (TOV) equation of state for dark matter fluids [103, 104]. The charged black hole systems solved from these dark matter models are more complex, and the $g_{tt} \times g_{rr} = -1$ relation for spacetime metric is no longer valid. The studies of more complex charged black hole solutions from dark matter model is beyond the scope of our present work.

3 Theoretical Methods to Obtain Gravitational Lensing Observables

This section gives descriptions on the theoretical methods used to calculate the gravitational lensing observables in our work. The treatments of particle orbits (which are geodesics) are presented in subsection 3.1. Schemes to obtain gravitational deflection angle of light and time delay of light for finite distance light source and observer are introduced in subsections 3.2 - 3.3. Finally, the formulations on the trajectories and precession angle for massive object's bound orbits around black holes are given in subsection 3.4.

3.1 Geodesics

In the gravitational field, massive and massless particles are moving along geodesics in 4 dimensional spacetime. Here we provide a derivation of the reduced geodesic equation, which turns out to be extremely useful in the exploration of gravitational lensing observables. For a spherically symmetric spacetime with the metric form

$$d\tau^2 = f(r)dt^2 - \frac{1}{f(r)}dr^2 - r^2(d\theta^2 + \sin^2\theta d\phi^2) \quad (8)$$

the following conserved quantities can be introduced from the symmetry and Killing vectors of spacetime

$$J \equiv r^2 \sin^2\theta \frac{d\phi}{d\lambda} \quad (9a)$$

$$E \equiv f(r) \frac{dt}{d\lambda} \quad (9b)$$

$$\epsilon \equiv g_{\mu\nu} dx^\mu dx^\nu = f(r) \left(\frac{dt}{d\lambda} \right)^2 - \frac{1}{f(r)} \left(\frac{dr}{d\lambda} \right)^2 - r^2 \left(\frac{d\theta}{d\lambda} \right)^2 - r^2 \sin^2\theta \left(\frac{d\phi}{d\lambda} \right)^2 \quad (9c)$$

Here, λ is an affine parameter in a particle orbit, J is the conserved angular momentum along the particle orbit, and $E^2/2$ can be viewed as the conserved energy along a particle orbit. Specifically, for spherically symmetric spacetime, we can always assume that test particles are moving in the equatorial plane $\theta = \pi/2$, and the reduced differential equation can be obtained using these conserved quantities

$$\frac{1}{2} \left(\frac{dr}{d\lambda} \right)^2 + \frac{1}{2} f(r) \left[\frac{J^2}{r^2} + \epsilon \right] = \frac{1}{2} \left(\frac{dr}{d\lambda} \right)^2 + V_{\text{eff}}(r) = \frac{1}{2} E^2 \quad (10)$$

Here, $V_{\text{eff}}(r) = \frac{f(r)}{2} \left[\frac{J^2}{r^2} + \epsilon \right]$ is the effective potential of test particles moving in a spherically symmetric gravitational field, and $b \equiv |J/E|$ is the impact parameter in a particle orbit (which is also conserved along this orbit). For massless particles traveling along null geodesics, the parameter ϵ takes the value $\epsilon = 0$. For massive particles traveling along timelike geodesics, the parameter ϵ takes the value $\epsilon = 1$.

3.2 Gravitational Deflection Angle of Light

The gravitational deflection angle reflects the bending or distortion effects on particle orbit in a gravitational field. In the gravitational lensing observation, when the light source and observer are located at a finite distance region to the central black hole (with the radial coordinate $r = r_S$ and $r = r_O$, respectively), the gravitational deflection angle of light is defined through [105]

$$\alpha \equiv \Psi_O - \Psi_S - \Delta\phi_{OS} \quad (11)$$

The notations Ψ_O , Ψ_S denote the angles between light ray propagation direction and the radial direction (which are measured at the observer's position and source position), and $\Delta\phi_{OS}$ is the variation of azimuthal angle ϕ in the light trajectory. For a spherically symmetric spacetime described by metric (8), the angle

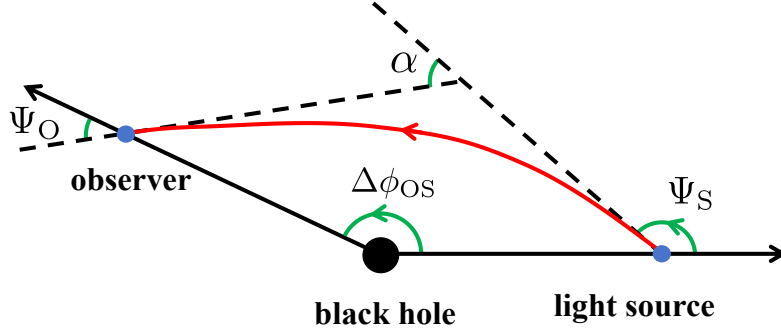


Figure 1: The gravitational deflection angle of light for finite distance light source and observer. This figure illustrate the gravitational deflection angle $\alpha \equiv \Psi_{\text{O}} - \Psi_{\text{S}} - \Delta\phi_{\text{OS}}$ in the thin lens approximation.

between light ray propagation direction and the radial direction is uniquely determined by spacetime metric [105], via

$$\sin \Psi = \frac{b \cdot \sqrt{f(r)}}{r} \quad (12)$$

The definition of gravitational deflection angle of light in expression (11) for finite distance light source and observer can be understood from an instructive way using thin lens approximation. In the thin lens approximation, the gravitational deflection angle for finite distance light source and observer is illustrated in figure 1. The thin lens approximation assumes that the spacetime is flat everywhere except for the location of gravitational thin lens (the central black hole position). For the quadrangle depicted in figure 1, the exterior angles at each point are Ψ_{S} , α , $\pi - \Psi_{\text{O}}$, $\pi - \Delta\phi_{\text{OS}}$, respectively. Under the thin lens approximation, the sum of exterior angles for the quadrangle equals 2π , which justify the definition of gravitational deflection angle $\alpha \equiv \Psi_{\text{O}} - \Psi_{\text{S}} - \Delta\phi_{\text{OS}}$. However, it should be noted that this definition in expression (11) given by Ishihara *et al.* is not restricted in the thin lens approximation. It is a consistent and proper definition of gravitational deflection angle that are hold in more generally gravitational lensing treatments (which can go beyond the thin lens approximation), see references [105–109] for more discussions on this issue.

To calculate the gravitational deflection angle of light, it is necessary to find the variation of azimuthal angle ϕ in the photon orbit. In a spherically symmetric spacetime, the variation of azimuthal angle ϕ is derived from the reduced differential equation (10) for null geodesics

$$\frac{d\phi}{dr} = \frac{d\phi}{d\lambda} \cdot \frac{d\lambda}{dr} = \pm \frac{1}{r^2 \sqrt{\frac{1}{b^2} - \frac{f(r)}{r^2}}} \quad (13)$$

where we have used the affine parameter $\epsilon = 0$ for massless photon, the conserved energy parameter $E = f(r) \frac{dt}{d\lambda}$, conserved angular momentum $J = r^2 \sin^2 \theta \frac{d\phi}{d\lambda}$, and the definition of impact parameter $b \equiv |J/E|$. The plus and minus sign \pm can be determined in the following way. When the photon beams travel along a scattering orbit from the source position r_{S} , the radial coordinate r decreases as the azimuthal angle ϕ increases, until photon beams reach the closet distance $r = r_0$ to central supermassive black hole. After passing the turning point $r = r_0$, the radial coordinate starts to increase with the increasing of azimuthal angle. This we derive the following relation

$$\begin{aligned} \frac{d\phi}{dr} &= -\frac{1}{r^2 \sqrt{\frac{1}{b^2} - \frac{f(r)}{r^2}}} < 0 && \text{from source position } r = r_{\text{S}} \text{ to tuning point } r = r_0 \\ \frac{d\phi}{dr} &= \frac{1}{r^2 \sqrt{\frac{1}{b^2} - \frac{f(r)}{r^2}}} > 0 && \text{from tuning point } r = r_0 \text{ to observer position } r = r_{\text{O}} \end{aligned}$$

For the closet distance to central black hole in the photon orbit, the derivative $dr/d\lambda$ in equation (10)

vanishes automatically

$$\begin{aligned} \left. \frac{dr}{d\lambda} \right|_{r=r_0} = 0 &\Rightarrow \frac{1}{2} f(r_0) \frac{J^2}{r_0^2} = \frac{1}{2} E^2 \\ &\Rightarrow b^2 = \frac{J^2}{E^2} = \frac{r_0^2}{f(r_0)} \end{aligned} \quad (15)$$

Given the impact parameter b for a photon orbit, the closet distance r_0 can be solved from this equation.

With the expression of angle Ψ in equation (12) and the variation of azimuthal angle, the gravitational deflection angle of light can be expressed as

$$\begin{aligned} \alpha &= \Psi_O - \Psi_S - \Delta\phi_{OS} \\ &= \Psi_O - \Psi_S + \int_{r_S}^{r_0} \frac{d\phi}{dr} dr + \int_{r_0}^{r_O} \frac{d\phi}{dr} dr \\ &= \arcsin\left(\frac{b\sqrt{f(r_R)}}{r_R}\right) + \arcsin\left(\frac{b\sqrt{f(r_S)}}{r_S}\right) - \pi + \int_{r_0}^{r_S} \frac{dr}{r^2 \sqrt{\frac{1}{b^2} - \frac{f(r)}{r^2}}} + \int_{r_0}^{r_O} \frac{dr}{r^2 \sqrt{\frac{1}{b^2} - \frac{f(r)}{r^2}}} \end{aligned} \quad (16)$$

As shown in figure 1, the angle Ψ measured at the position of light source is an obtuse angle such that $\Psi_S = \pi - \arcsin\left(\frac{b\sqrt{f(r_S)}}{r_S}\right)$.

3.3 Time Delay of Light

In the gravitational field, the elapse of time (measured by an observer) during the light propagation can be strongly affected by gravitation, and this is the time delay effect of gravitational field. To calculate the time delay of light in gravitational lensing observations, it is necessary to compute the variation of time coordinate t (measured by an distant observer) in the photon orbit. For the massless photon traveling along null geodesics (with $\epsilon = 0$), one can derive the time derivative of radial coordinate from the reduced geodesic equation in (10)

$$\frac{dr}{dt} = \frac{dr}{d\lambda} \cdot \frac{d\lambda}{dt} = \pm f(r) \sqrt{1 - b^2 \cdot \frac{f(r)}{r^2}} \quad (17)$$

The plus and minus sign \pm can be determined similar to the calculation of gravitational deflection angle. When the photon beams are emitted from the source position r_S , the radial coordinate r decreases as time passes, until the photon beams reach the closet distance $r = r_0$ to central supermassive black hole. After passing the turning point $r = r_0$, the radial coordinate starts to increase as time advances. So we have the relation

$$\begin{aligned} \frac{dt}{dr} &= -\frac{1}{f(r) \sqrt{1 - b^2 \cdot \frac{f(r)}{r^2}}} < 0 \quad \text{from source position } r = r_S \text{ to tuning point } r = r_0 \\ \frac{dt}{dr} &= \frac{1}{f(r) \sqrt{1 - b^2 \cdot \frac{f(r)}{r^2}}} > 0 \quad \text{from tuning point } r = r_0 \text{ to observer position } r = r_O \end{aligned}$$

In the gravitational lensing observation, when the light source and observer are located at $r = r_S$ and $r = r_O$, the time delay of light during the light propagation process can be expressed as

$$\begin{aligned} \Delta T = T - T_0 &= \int_{r_S}^{r_0} \frac{dt}{dr} dr + \int_{r_0}^{r_O} \frac{dt}{dr} dr - T_0 \\ &= -\int_{r_S}^{r_0} \frac{dr}{f(r) \sqrt{1 - \frac{b^2 f(r)}{r^2}}} + \int_{r_0}^{r_O} \frac{dr}{f(r) \sqrt{1 - \frac{b^2 f(r)}{r^2}}} - T_0 \\ &= \int_{r_0}^{r_S} \frac{dr}{f(r) \sqrt{1 - \frac{b^2 f(r)}{r^2}}} + \int_{r_0}^{r_O} \frac{dr}{f(r) \sqrt{1 - \frac{b^2 f(r)}{r^2}}} - \sqrt{r_S^2 - r_0^2} - \sqrt{r_O^2 - r_0^2} \end{aligned} \quad (19)$$

with $T_0 = \sqrt{r_S^2 - r_0^2} + \sqrt{r_O^2 - r_0^2}$ to be the time period during the light propagation process without the gravitational field. In the expression (19), it is obvious that the time delay ΔT increases monotonically as

the coordinates of light source and observer r_S, r_O increase. Additionally, in the integration, the turning point $r = r_0$ is solved through equation (15).

Furthermore, it should be addressed that the time delay of light calculated using expression (19) is the time delay measured by the conventional static time coordinate t in spacetime metric expression (8). For an asymptotically flat spacetime, the static time coordinate corresponds to the time measured by a very distant observer (at the asymptotically flat region). On the other hand, if one wants to calculate the time delay measured by the proper time of a finite distance static observer, a redshift factor should be taken into account

$$\Delta T_{\text{static observer's proper time unit}} = \frac{\Delta T}{\text{redshift factor}} = \frac{\Delta T}{\sqrt{f(r_O)}} \quad (20)$$

with r_O to be the position of finite distance static observer.

3.4 Massive Object's Orbits and Precession Angle

Besides the gravitational deflection angle and time delay of light discussed in subsections 3.2-3.3 (which is relevant to a scattering orbit for massless photons), the massive object's orbits are also greatly influenced by gravitational field, both for bound orbits and scattering orbits. Notably, massive object's bound orbits may exhibit precession. In the gravitational lensing observations, the precession of bound orbits is frequently used to test the gravitational field around the supermassive black hole in galaxy center (such as the observations relevant to Sgr*A in Milky Way Galaxy).

For a spherically symmetric black hole spacetime, we can always restrict the motion of massive object's in the equatorial plane. To calculate the massive object's orbit in the equatorial plane, it is necessary to resort to the reduced geodesic equation (10) and the definition of conserved momentum

$$\left(\frac{dr}{d\tau}\right)^2 = E^2 - V_{\text{eff}}(r) = E^2 - f(r) \left[\frac{J^2}{r^2} + 1\right] \quad (21a)$$

$$\frac{d\phi}{d\tau} = \frac{J}{r^2} \quad (21b)$$

where we have used the proper time as the affine parameter for massive objects traveling along timelike geodesics. The parameter ϵ takes the value $\epsilon = 1$ for timelike geodesics. Substitute the expression (21b) into equation (21a) and cancel the affine parameter τ , the geodesic equation can be further reduced to

$$\begin{aligned} \left(\frac{dr}{d\phi} \frac{J}{r^2}\right)^2 &= E^2 - V_{\text{eff}}(r) = E^2 - f(r) \left[\frac{J^2}{r^2} + 1\right] \\ \Rightarrow \left(\frac{du}{d\phi}\right)^2 &= \frac{1}{b^2} - F(u) \left[u^2 + \frac{1}{J^2}\right] \end{aligned} \quad (22)$$

where we have used the new variable $u = 1/r$ in the geodesic equation. Differentiating each side of this equation with respect to ϕ , a second order differential equation for massive object's orbit can be obtained

$$\frac{d^2u}{d\phi^2} = -\frac{1}{2} \cdot \frac{dF(u)}{du} \cdot \left[u^2 + \frac{1}{J^2}\right] - F(u) \cdot u \quad (23)$$

The function $F(u) = f(1/r)$ is the spacetime metric component expressed using new variable $u = 1/r$. Eventually, the massive object's orbit is determined by numerically solving the differential equation (23).

An important feature of the massive object's bound orbit is the precession of azimuthal angle ϕ , which is illustrated in figure 2. Given a bound timelike geodesic orbit for a massive object, there are maximal and minimal distance positions to central black hole in this orbit, denoting as r_{max} and r_{min} . The precession of azimuthal angle ϕ in an orbit period can be calculated as

$$\begin{aligned} \Delta\phi_{\text{precession}} &= \int_{r_{\text{min}}}^{r_{\text{max}}} \frac{d\phi}{dr} dr + \int_{r_{\text{max}}}^{r_{\text{min}}} \frac{d\phi}{dr} dr - 2\pi \\ &= 2 \int_{r_{\text{min}}}^{r_{\text{max}}} \frac{dr}{r^2 \sqrt{\frac{1}{b^2} - \frac{f(r)}{r^2} - \frac{f(r)}{J^2}}} - 2\pi \end{aligned} \quad (24)$$

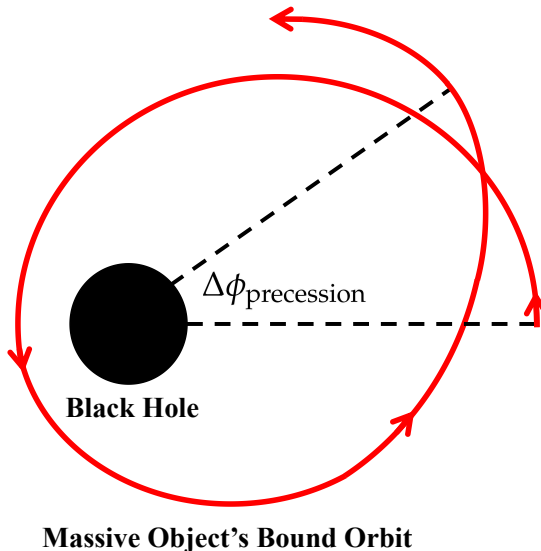


Figure 2: A schematic plot of the precession of azimuthal angle for a massive object's bound orbit around the central black hole.

In the derivation of precession angle $\Delta\phi_{\text{precession}}$, we have used the derivative of azimuthal angle with respect to radial coordinate for a timelike geodesic orbit

$$\frac{d\phi}{dr} = \frac{d\phi}{d\tau} \cdot \frac{d\tau}{dr} = \pm \frac{1}{r^2 \sqrt{\frac{1}{b^2} - \frac{f(r)}{r^2} - \frac{f(r)}{J^2}}} \quad (25)$$

The plus and minus sign \pm can be determined as follows. When a massive object begins to move along timelike geodesics from the maximal distance position r_{max} , the radial coordinate r decreases as azimuthal angle ϕ increases, until the massive object reaches the minimal distance position $r = r_{\text{min}}$ to central supermassive black hole. After passing the minimal distance position $r = r_{\text{min}}$, the massive object's radial coordinate starts to increase as azimuthal angle increases. Thus we can get the relation

$$\begin{aligned} \frac{d\phi}{dr} &= -\frac{1}{r^2 \sqrt{\frac{1}{b^2} - \frac{f(r)}{r^2} - \frac{f(r)}{J^2}}} < 0 && \text{from maximal distance } r = r_{\text{max}} \text{ to minimal distance } r = r_{\text{min}} \\ \frac{d\phi}{dr} &= \frac{1}{r^2 \sqrt{\frac{1}{b^2} - \frac{f(r)}{r^2} - \frac{f(r)}{J^2}}} > 0 && \text{from minimal distance } r = r_{\text{min}} \text{ to maximal distance } r = r_{\text{max}} \end{aligned}$$

Furthermore, the maximal and minimal distance position to the central black hole in a massive object's bound orbit can be determined via

$$\left. \frac{dr}{d\phi} \right|_{r=r_{\text{max}}, r=r_{\text{min}}} = r^2 \sqrt{\frac{1}{b^2} - \frac{f(r)}{r^2} - \frac{f(r)}{J^2}} \Big|_{r=r_{\text{max}}, r=r_{\text{min}}} = 0 \quad (27)$$

4 Results and Discussions

This section presents results on the gravitational lensing observables for Euler-Heisenberg black hole surrounded by PFDM, including the gravitational deflection angle of light, time delay of light, the trajectory and precession angle of massive object's bound orbits. These results are calculated numerically using expressions (16), (19) and (23). Furthermore, inspired by the rapid development of black hole shadow researches since the capture of black hole images by ETH, we also present a discussion on the black hole shadow for Euler-Heisenberg black hole surrounded by PFDM.

4.1 Gravitational Deflection Angle of Light

The gravitational deflection angle of light for Euler-Heisenberg black hole surrounded by PFDM are given in figure 3. They are calculated numerically from expression (16) for light source and observer located at finite distance region. In figure 3, the upper left and upper right panels highlight the influences from black hole electric charge Q and the nonlinear electrodynamics effects / QED effects (parameterized by a), while the lower panels highlight the influences from dark matter parameterized by λ_{DM} . To show the gravitational deflection in strong gravitational field cases, the minimal value of impact parameter is chosen as $b \sim 10M$, which indicates the photon orbit is very close to the black hole critical shadow radius.

The upper left panel of figure 3 suggests that, for a constant PFDM parameter and nonlinear electrodynamics parameter, the gravitational deflection angles are slightly reduced when black hole's electric charge become larger. But the effect coming from electric charge is small such that we must add a magnified subplot into upper left panel to separate the various curves corresponding to different black hole charges. The upper right panel of figure 3 suggests that the nonlinear electrodynamics parameter has no obvious influences on the gravitational deflection angles, even if a magnified subplot is employed. Comparing the upper and lower panels of figure 3, we can observe that both electric charge and nonlinear electrodynamics have minor impacts on gravitational deflection angle, while the most significant influences coming from the PFDM. From the lower panels of figure 3, it can be clearly manifested that the variation of PFDM parameter could dramatically change the gravitational deflection angle of light for charged Euler-Heisenberg black hole. Notably, the gravitational deflection angle reduce rapidly as the increasing of PFDM parameter λ_{DM} . This can be explained from the spacetime metric in expression (6) for Euler-Heisenberg black hole surrounded by PFDM. The dark matter effects contribute to the spacetime metric function $f(r)$ via the $-\lambda_{\text{DM}}/r$ term (if we naively omit the slowly varying logarithmic term $\ln \frac{r}{|\lambda_{\text{DM}}|}$ for simplicity), which is similar to the black hole's mass term $2M/r$. This indicates that the PFDM parameter could play a role of "effective mass" in the spacetime metric¹. A positive PFDM parameter ($\lambda_{\text{DM}} > 0$) contributes to a negative effective mass in the spacetime metric, which explains the rapid drop of the gravitational deflection angle when PFDM parameter becomes larger. Furthermore, combining the four panels of figure 3, it is also interesting to find that the gravitational deflection angles of light for Euler-Heisenberg black hole surrounded by PFDM (with nonzero electric charge $Q \neq 0$ and dark matter parameter $\lambda_{\text{DM}} \neq 0$) are smaller than those in Schwarzschild black hole cases (which correspond to the black solid line in the lower left panel of figure 3).

4.2 Time Delay of Light

The time delay results for Euler-Heisenberg black hole surrounded by PFDM are presented in figure 4. This figure plots the time delay of light measured by the conventional static time coordinate t in spacetime metric (8). They are obtained numerically from expression (19) for light source and observer located at a finite distance region. In this figure, the time delays of light varied with respect to light source position r_{S} are plotted. A similar plot can be carried out for time delays varied with respect to observer position r_{O} , while these results exhibit very similar behaviors with those in figure 4. So the plot of time delays varied with respect to observer position is not given in this work. In figure 4, the upper left and upper right panels highlight the influences from black hole electric charge Q and the nonlinear electrodynamics effects (or QED effects) parameterized by a , while the lower panels highlight the influences from dark matter parameterized by λ_{DM} . In all four panels, the time delays of light all grow with the increasing of light source radius r_{S} , confirming that the time delay of light ΔT calculated using expression (19) is indeed a monotonically function of light source radius r_{S} (or observer radius r_{O}).

Comparing the time delay results in figure 4 and the gravitational deflection results in figure 3, it is easy to observe that the black hole parameters (including the black hole electric charge Q , nonlinear electrodynamics parameter a , PFDM parameter λ_{DM}) influence time delays of light in a similar trend as those for gravitational deflection angles. Firstly, Euler-Heisenberg black hole with a larger electric charge results in a reduction of time delay, as shown in the upper left panel of figure 4. Secondly, the nonlinear electrodynamics effects (parameterized by a) do not have obvious influences on time delay results, as indicated in the upper right panel of figure 4. Thirdly, the most significant impacts on time delay coming from the PFDM, which are much greater than those from electric charge and nonlinear electrodynamics. From the lower panels of figure 4, the time delay of light changes rapidly as the PFDM parameter varies. Particularly, the time delay of light could undergo a rapid reduction for larger PFDM parameters, compared with those in the absence of dark

¹Strictly speaking, because of the presence of logarithmic term, this "effective mass" should be $m_{\text{eff}}(r) = \lambda_{\text{DM}} \ln \frac{r}{|\lambda_{\text{DM}}|}$, rather than $m_{\text{eff}} = \lambda_{\text{DM}}$.

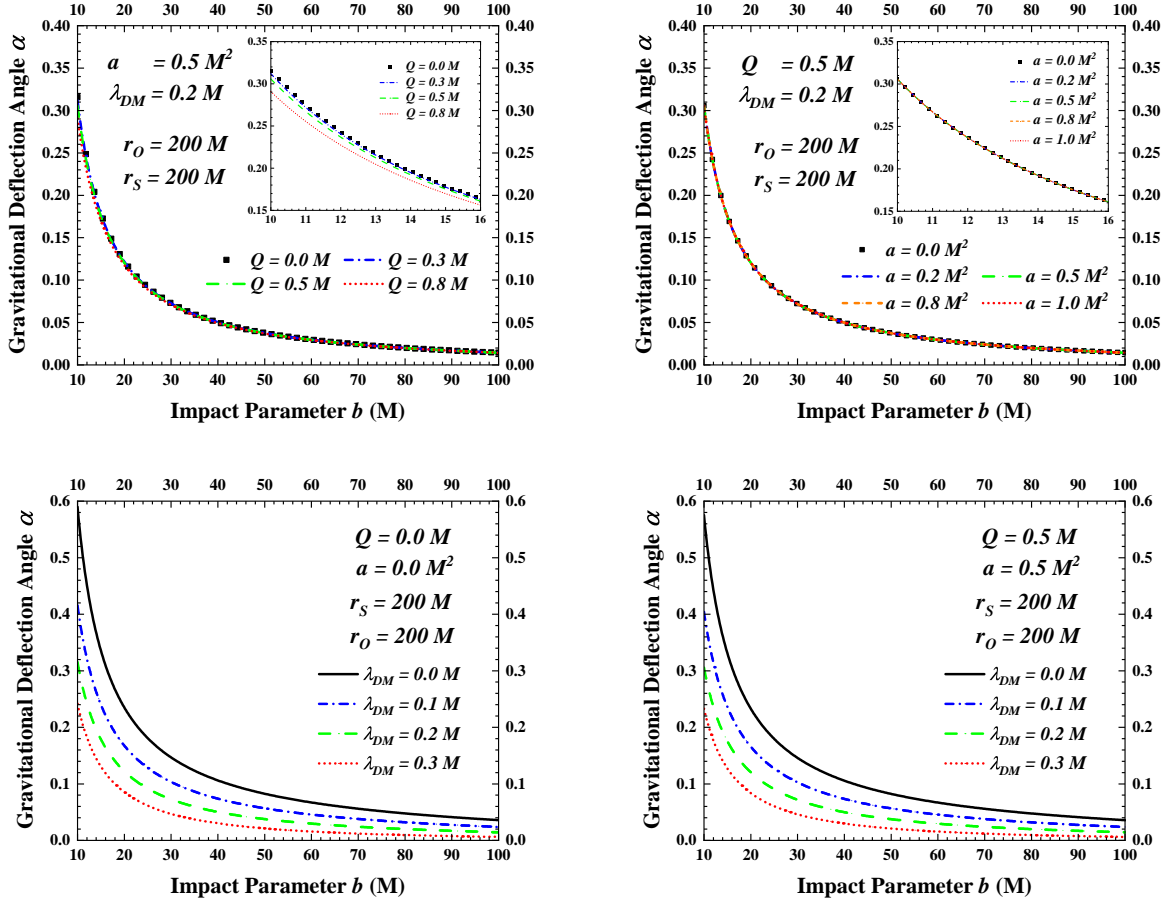


Figure 3: The gravitational deflection angle of light for Euler-Heisenberg black hole surrounded by PFDM. The gravitational deflection angles are calculated numerically from expression (16) for finite distance light source and observer. This figure highlights the influences of black hole electric charge, nonlinear electrodynamics effects and dark matter effects on gravitational deflection angles. (a) The upper left panel exhibits the influences from black hole electric charge Q , with the nonlinear electrodynamics parameter $a = 0.5M^2$ and PFDM parameter $\lambda_{\text{DM}} = 0.2M$. (b) The upper right panel shows the influences from nonlinear electrodynamics effects / QED effects, with the black hole charge $Q = 0.5M$ and PFDM parameter $\lambda_{\text{DM}} = 0.2M$. (c) The lower left panel highlights the influences from dark matter in the absence of electric charge and nonlinear electrodynamics effects (with $Q = 0$ and $a = 0$). (d) The lower right panel highlights the influences from dark matter in the presence of nonlinear electrodynamics effects, with the black hole charge $Q = 0.5M$ and nonlinear electrodynamics parameter $a = 0.5M^2$. In all four panels of this figure, the horizontal axis labels the impact parameter in photon orbit, which is increased from $b = 10M$ to $b = 100M$. The position of light source and observer are located at a certain distance $r_{\text{O}} = r_{\text{S}} = 200M$.

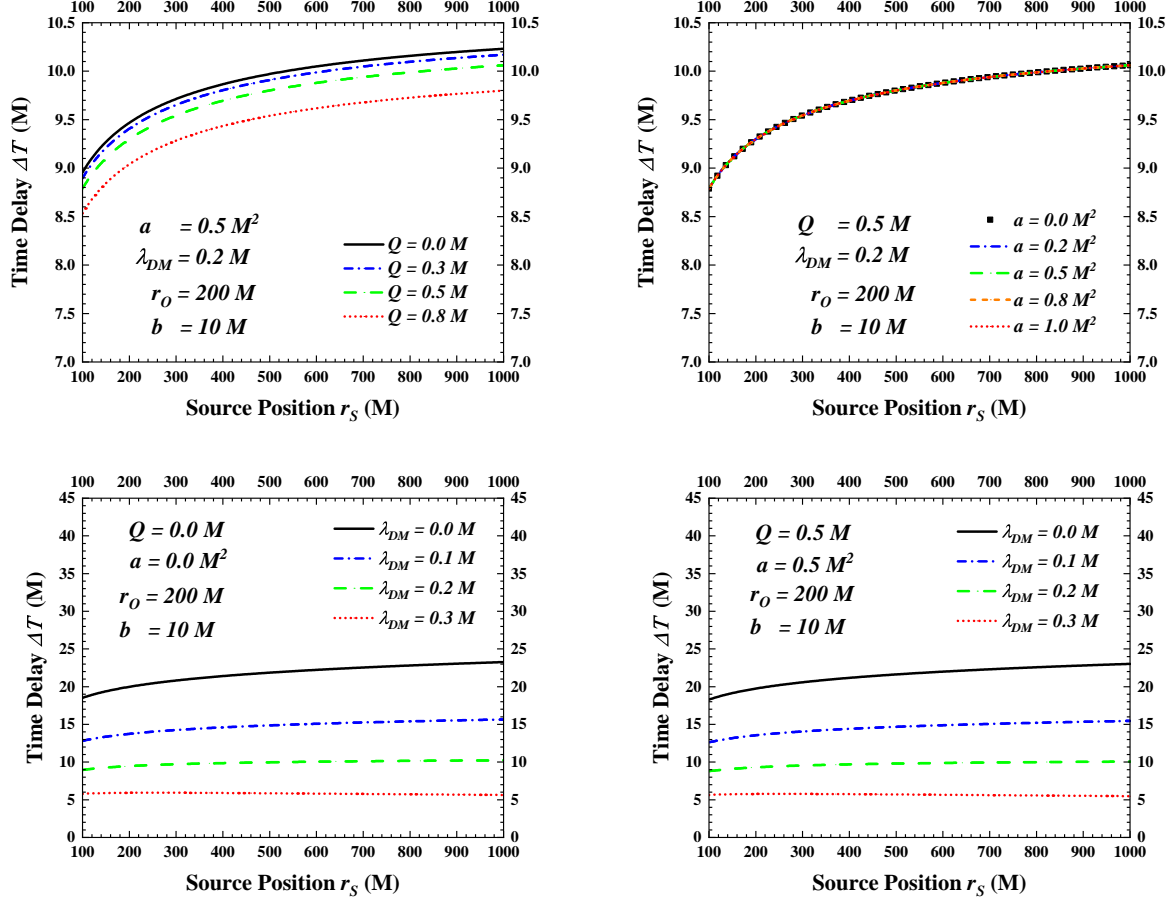


Figure 4: The gravitational time delay of light for Euler-Heisenberg black hole surrounded by PFDM. The time delays of light (which are measured by the conventional static time coordinate t) are calculated numerically from expression (19) for finite distance light source and observer. This figure plots the time delay results, highlighting the influences coming from various black hole parameters. (a) The upper left panel shows the influences from black hole electric charge Q , with the nonlinear electrodynamics parameter $a = 0.5M^2$ and dark matter parameter $\lambda_{\text{DM}} = 0.2M$. (b) The upper right panel exhibits the influences from nonlinear electrodynamics effects / QED effects, with the black hole charge $Q = 0.5M$ and PFDM parameter $\lambda_{\text{DM}} = 0.2M$. (c) The lower left panel highlights the influences from dark matter in the absence of black hole charge and nonlinear electrodynamics effects (with $Q = 0$ and $a = 0$). (d) The lower right panel highlights the influences from dark matter in the presence of nonlinear electrodynamics effects, with the black hole charge $Q = 0.5M$ and nonlinear electrodynamics parameter $a = 0.5M^2$. In all four panels of this figure, the horizontal axis labels the position of light source varied from $r_S = 100M$ to $r_S = 1000M$, and the vertical axis labels the time delay of light ΔT in unit of black hole mass. The position of observer is chosen to be $r_O = 200M$, and the impact parameter in photon orbit satisfies $b = 10M$.

Table 1: The local minimum position of effective potential for massive objects moving around Euler-Heisenberg black hole in the presence of PFDM. In this table, the black hole electric charge and nonlinear electrodynamics parameter are chosen to be $Q = 0.5M$, $a = 0.5M^2$, and conserved angular momentum for massive object's bound orbit is selected as $J = 4M$. In this table, we have substituted $1/2$ in the effective potential given in equation (10) such that the effective potential for massive object vanished in the asymptotic flat region (the infinity) $\lim_{r \rightarrow \infty} V_{\text{eff}}(r) = \lim_{r \rightarrow \infty} \left\{ \frac{f(r)}{2} \left[\frac{J^2}{r^2} + \epsilon \right] - \frac{1}{2} \right\} = 0$.

PFDM parameter	$\lambda_{\text{DM}} = 0.0M$	$\lambda_{\text{DM}} = 0.05M$	$\lambda_{\text{DM}} = 0.1M$	$\lambda_{\text{DM}} = 0.2M$
local minimum of V_{eff}	$V_{\text{min}} = -0.03611$	$V_{\text{min}} = -0.02539$	$V_{\text{min}} = -0.01807$	$V_{\text{min}} = -0.00821$

matter (with $\lambda_{\text{DM}} = 0$). This can be explained by the ‘‘effective mass’’ role of PFDM played in the spacetime metric, the same as we have elaborated in subsection 4.1 for gravitational deflection angle cases. A positive PFDM parameter $\lambda_{\text{DM}} > 0$ contributes to a negative effective mass in the spacetime metric, which explains the rapid reduction of time delay for larger PFDM parameter values. Furthermore, combining the four panels of figure 4, it is worth noting that the time delays of light for Euler-Heisenberg black hole surrounded by PFDM (with nonzero electric charge $Q \neq 0$ and dark matter parameter $\lambda_{\text{DM}} \neq 0$) are smaller than those in Schwarzschild black hole cases (which correspond to the black solid line in the lower left panel of figure 4).

4.3 Massive Object's Bound Orbits and Precession Angle

The figure 5 displays numerical results on massive object's bound orbits around the Euler-Heisenberg black hole surround by PFDM, including the precession angles in the left panels and the trajectories of orbits in the right panels. The trajectories of massive object's orbits are obtained by numerically solving the ordinary differential equation (23), and the precession angles of orbits are calculated from the integral in expression (24). The upper, middle and lower panels of figure 5 highlight the influences from black hole electric charge, dark matter (parameterized by PFDM parameter λ_{DM}), and nonlinear electrodynamics effects / QED effects (parameterized by nonlinear electrodynamics parameter a) correspondingly. In this figure, we present results on the trajectory of orbits and their precession angles for a selected angular momentum value $J = 4M$. The variation trend of precession angles correspond to other angular momentum values is similar to that for $J = 4M$ presented in figure 5².

The results in figure 5 show that both black hole electric charge and PFDM can intensely influence the precession angle of massive object's orbits in the vicinity of Euler-Heisenberg black hole. The upper panels of figure 5 suggests that a larger black hole charge reduces the precession angle of orbits. However, unlike the precession angle, the shape of massive object's bound orbits are not violently influenced by black hole electric charge. In the upper right panel of figure 5, the shape and eccentricity of massive object's orbits calculated for different black hole charge values do not exhibit large differences, until the electric charge grows to a value closer the extreme black hole cases (see the $Q = 0.8M$ case, which corresponds to the dotted line in the upper right panel). On the other hand, the middle panels indicate that the PFDM have great impacts not only on the precession angle of orbits, but also on the shape of massive object's bound orbits. The middle left panel tells that a larger PFDM parameter can significantly reduce the precession angle of bound orbits. The middle right panel shows that the shape, eccentricity and semimajor-axis length of massive object's bound orbits exhibit notable differences when PFDM parameter takes different values. Moreover, in the middle left panel, the proper region for energy parameter $\epsilon_{\text{energy}} = \frac{E^2 - 1}{2}$ which allows the existence of bound orbits is also reduced with the increasing of PFDM parameter. This is caused by the local minimum position of effective potential for massive objects. For any massive object's bound orbits with precession, the total energy ϵ_{energy} in this orbit must exceed the local minimum of effective potential. The local minimum values of effective potential for massive objects moving around Euler-Heisenberg black hole in the presence of PFDM (for a selected angular momentum value $J = 4M$ and several PFDM parameter values) are listed in table 1. Furthermore, unlike the black hole electric charge and PFDM, the nonlinear electrodynamics effects / QED effects (parameterized by a) have very tiny impacts on the trajectories of massive object's orbits and their precession angles, which can be directly observed from the lower panels of figure 5. This trend is similar to the cases of gravitational deflection and time delay, where the nonlinear electrodynamics effects also produce very tiny influences on these gravitational lensing observables.

²For other angular momentum values, the proper region for conserved energy where bound orbits of massive objects could exist is different from those in figure 5.

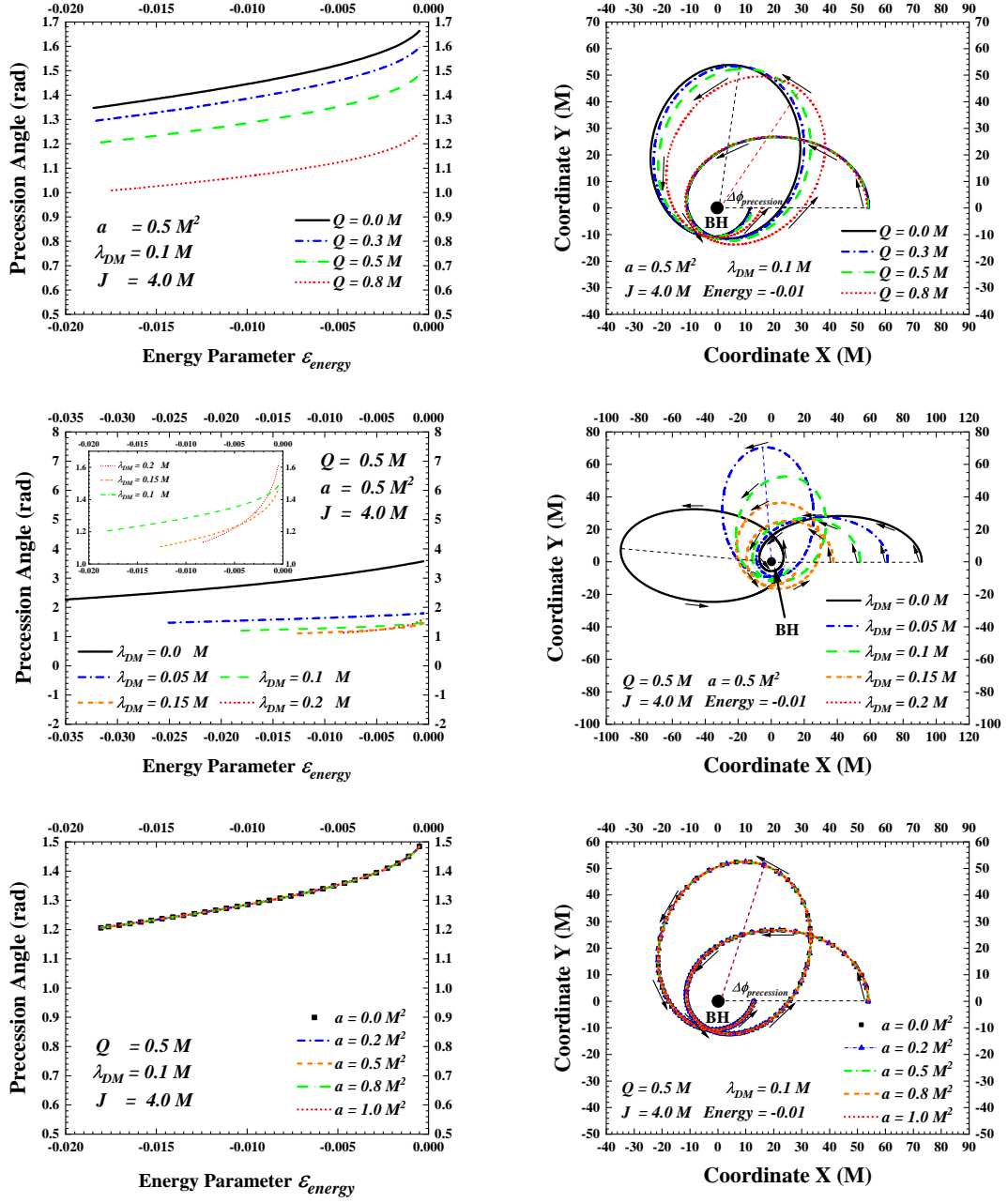


Figure 5: The precession angles and trajectories of massive particle's bound orbits moving around the Euler-Heisenberg black hole in the presence of PFDM. The precession angles $\Delta\phi_{\text{precession}}$ plotted in this figure are calculated numerically from expression (24) for a given conserved angular momentum value, and the trajectories of orbits are obtained by numerically solving the differential equation (23). The left panels shows the variation of precession angle as the changes of total energy parameter $\epsilon_{\text{energy}} = \frac{E^2 - 1}{2}$, while the right panels illustrate the trajectories of particle orbits (It should be noted that we have substituted $1/2$ in the both side of equation (10) such that the energy parameter vanished at infinity, namely $\lim_{r \rightarrow \infty} \epsilon_{\text{energy}} = 0$). (a) The upper left panel plots the precession angle of orbits affects by black hole charge Q . (b) The upper right panel illustrates the trajectories of orbits for different black hole charge values when total energy equals to $\epsilon_{\text{energy}} = -0.01$ (c) The middle left panel shows the precession angle of orbits affects by dark matter (parameterized by λ_{DM}). (d) The middle right panel illustrates the trajectories of orbits for different PFDM parameter values with total energy to be $\epsilon_{\text{energy}} = -0.01$ (however, in the case of $\lambda_{\text{DM}} = 0.2M$, the bound orbit does not exist because the local minimum of effective potential $V_{\text{min}} < \epsilon_{\text{energy}} = -0.01$, see table 1) (e) The lower left panel shows the precession angle of orbits influenced by nonlinear electrodynamics effects / QED effects (parameterized by a). (f) The lower right panel illustrates the trajectories of orbits for different nonlinear electrodynamics parameter values with total energy to be $\epsilon_{\text{energy}} = -0.01$.

4.4 Black Hole Shadow

This subsection discusses the black hole shadow for Euler-Heisenberg black hole surrounded by PFDM. The critical shadow radius of a black hole is determined by the unstable photon sphere, which can be calculated from the effective potential of photons moving in gravitational field, or through a geometric approach proposed in a recent works [110]. Here, we calculate the radius of unstable photon sphere and the black hole shadow radius based on the geometric approach, in which the photon sphere and its stability are uniquely determined from Gaussian curvature and geodesic curvature in the optical geometry of black hole spacetime. Firstly, any photon orbits maintain their geodesic nature when they are transformed into optical geometry, so the geodesic curvature for a photon sphere vanishes. This geodesic curvature condition for photon sphere is completely equivalent to find the local extreme point of effective potential [110–112]

$$\kappa_g(r = r_{\text{ph}}) = 0 \Leftrightarrow \left. \frac{dV_{\text{eff}}(r)}{dr} \right|_{r=r_{\text{ph}}} = 0 \quad (28)$$

Furthermore, the unstable photon spheres (or stable photon spheres) are determined by the negative (or positive) sign of Gaussian curvature, which is equivalent to find the local maximum (or local minimum) points of effective potential [110–112]

$$\mathcal{K}(r = r_{\text{unstable}}) < 0 \Leftrightarrow \left. \frac{d^2V_{\text{eff}}(r)}{dr^2} \right|_{r=r_{\text{unstable}}} < 0 \quad (29a)$$

$$\mathcal{K}(r = r_{\text{stable}}) > 0 \Leftrightarrow \left. \frac{d^2V_{\text{eff}}(r)}{dr^2} \right|_{r=r_{\text{stable}}} > 0 \quad (29b)$$

The absolute apparent size of black hole shadow viewed by an observer located at infinity (the asymptotically flat region) is characterized by critical shadow radius. With the unstable photon sphere obtained in equations (28) and (29a), the critical shadow radius of a black hole can be calculated through the relation

$$r_{sh} = b_{\text{critical}} = \frac{r_{\text{unstable}}}{\sqrt{f(r = r_{\text{unstable}})}} \quad (30)$$

The numerical results on black hole shadow for Euler-Heisenberg black hole surrounded by PFDM are presented in figure 6. The left panels plot the critical shadow radius r_{sh} calculated using expression (30), and the right panels illustrate the black hole shadow in celestial coordinates, highlighting the black hole shadow affected by three black hole parameters (the black hole electric charge Q , PFDM parameter λ_{DM} and nonlinear electrodynamics parameter a). From figure 6, it is reasonable to draw the following conclusions. Firstly, the increasing of black hole electric charge diminishes the apparent size of black hole shadow. Secondly, the lower left panel shows that the nonlinear electrodynamics parameter a has very tiny influences on the black hole shadow size. For the same electric charge and PFDM parameter, the critical shadow radius calculated with different nonlinear electrodynamics parameter values do not exhibit any obvious differences. Thirdly, when PFDM parameter is not vary large, such as $\lambda_{\text{DM}} \leq 0.5M$ in upper and middle panels of figure 6, the size of black hole shadow is enlarged as PFDM parameter reduced. However, this statement is no longer valid when PFDM reaches a large critical point, see figure 7.

To further explore the dark matter effects on black hole shadow size, we use figure 7 to show the critical shadow radius changed with respect to PFDM parameter, both in the presence and absence of nonlinear electrodynamics effects. It can be observed that when PFDM parameter is smaller than a critical value ($\lambda_{\text{DM}} < \lambda_{\text{critical}}$), the black hole shadow radius reduces with the increasing of PFDM parameter. However, when PFDM parameter exceeds this critical value ($\lambda_{\text{DM}} > \lambda_{\text{critical}}$), the black hole shadow radius get magnified as the increasing of PFDM parameter. This seems to be a universal properties of the PFDM effects on black hole shadows. Recent studies on charged RN black hole surrounded by PFDM have reported similar conclusions as we have presented here (the existence of critical point $\lambda_{\text{critical}}$) [48–50]. Furthermore, figure 7 shows that the critical value of PFDM parameter is roughly $0.5M < \lambda_{\text{critical}} < 0.8M$ for different black hole charge values. Since the nonlinear electrodynamics effects have tiny influences on black hole shadow size, the left and right panels of figure 7 exhibit very similar results and trends.

Interestingly, the black hole shadow results for Euler-Heisenberg black hole surrounded by PFDM in the presence and absence of nonlinear electrodynamics effects / QED effects could also exhibit a slight difference. In the absence of nonlinear electrodynamics effects, because of the emergence of naked singularity when black hole charge $Q > Q_{\text{extreme}}$, the black hole shadow disappears for large black hole electric charge. On

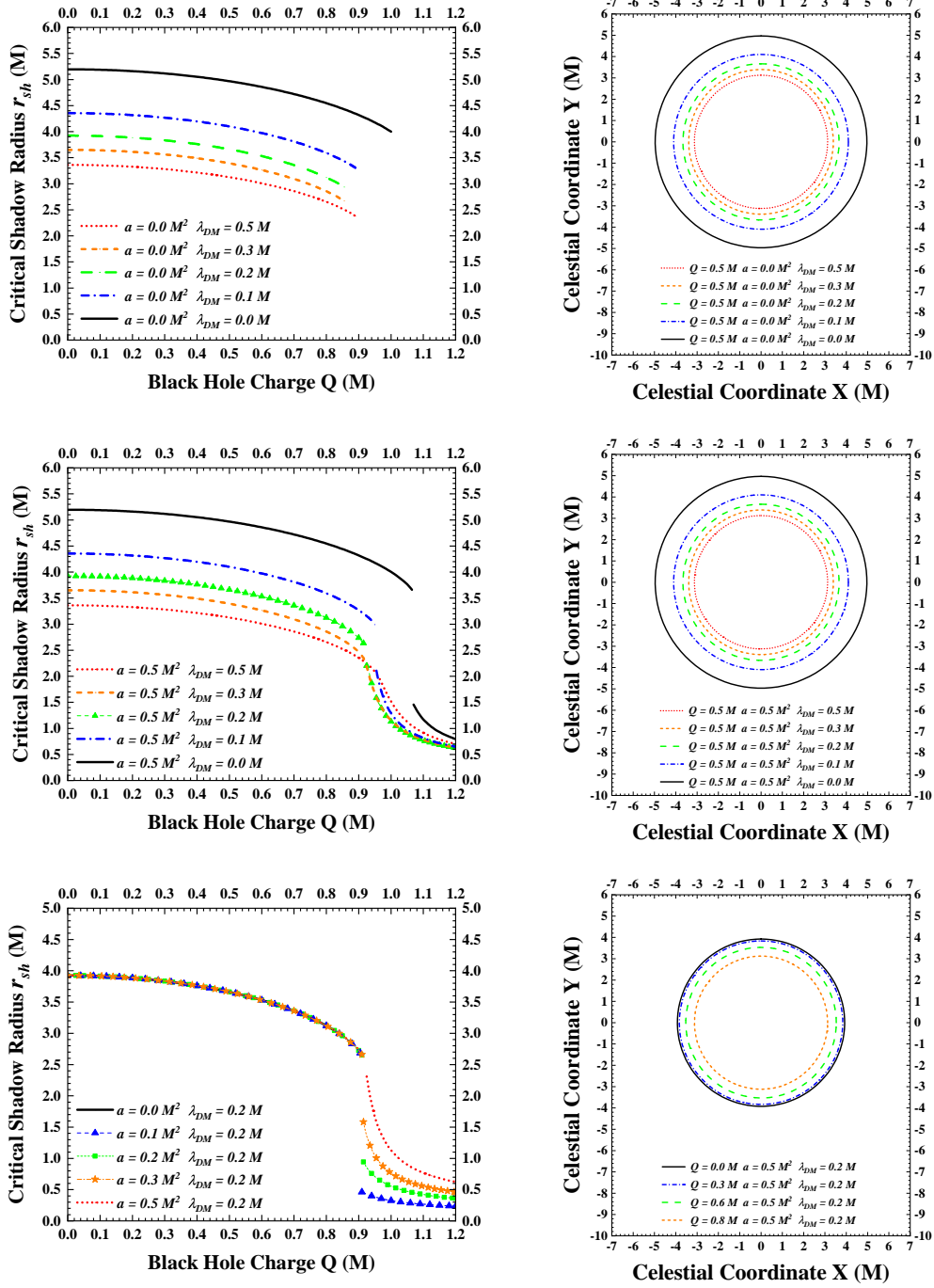


Figure 6: The black hole shadow of Euler-Heisenberg black hole surrounded by PFDM. The multiple panels of this figure highlight the influences coming from black hole electric charge, dark matter effects and nonlinear electrodynamics effects. (a) The upper left panel shows the critical shadow radius affected by PFDM in the absence of nonlinear electrodynamics effects (with $a = 0$). (b) The upper right panel illustrates the black hole shadow in celestial coordinates affected by PFDM in the absence of nonlinear electrodynamics effects (with $a = 0$ and $Q = 0.5M$). (c) The middle left panel shows the critical shadow radius affected by PFDM in the presence of nonlinear electrodynamics effects (with $a = 0.5M^2$). (d) The middle right panel illustrates the black hole shadow in celestial coordinates affected by PFDM in the presence of nonlinear electrodynamics effects (with $a = 0.5M^2$ and $Q = 0.5M$). (e) The lower left panel presents the critical shadow radius influenced by nonlinear electrodynamics effects (with $\lambda_{DM} = 0.2M$). (f) The lower right panel shows the black hole shadow in celestial coordinates influenced by black hole electric charge (with $a = 0.5M^2$ and $\lambda_{DM} = 0.2M$). In all panels of this figure, the black hole shadow radius r_{sh} , black hole electric charge Q , PFDM parameter λ_{DM} and nonlinear electrodynamics parameter a are given in unit of black hole mass M .

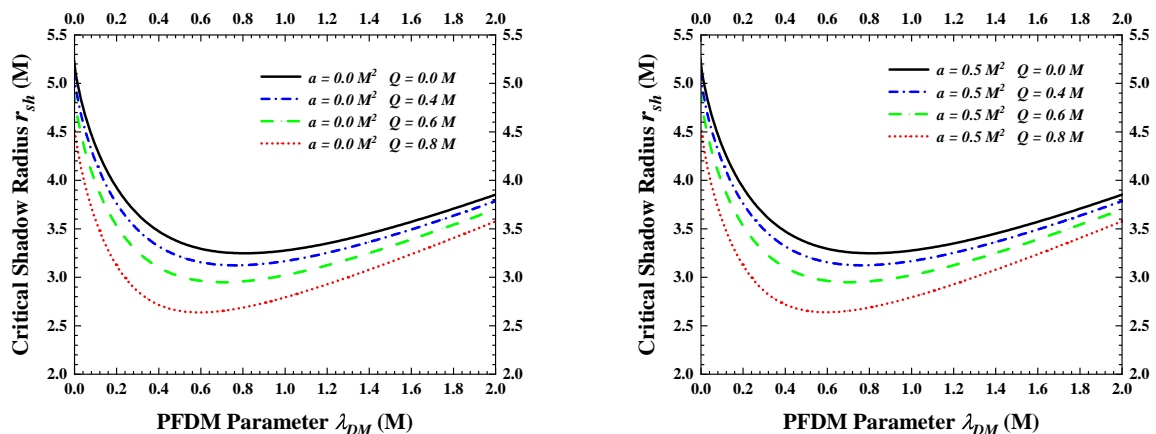


Figure 7: The black hole shadow of Euler-Heisenberg black hole surrounded by PFDM. This figure exhibits the variation of black hole critical shadow radius with respect to PFDM parameter. (a) The left panel shows the critical shadow radius for Euler-Heisenberg black hole surrounded by PFDM in the absence of nonlinear electrodynamics effects (with $a = 0$). (b) The right panel shows the critical shadow radius for Euler-Heisenberg black hole surrounded by PFDM in the presence of nonlinear electrodynamics effects (with $a = 0.5M^2$).

the other hand, in the presence of nonlinear electrodynamics effects, although the Euler-Heisenberg black hole (surrounded by PFDM) do not produce any naked singularities (see Appendix A for the discussions on horizons), the black hole shadow may still disappear under some circumstances. In the middle left panel of figure 6, when PFDM parameter takes the values $\lambda_{\text{DM}} = 0.0M, 0.1M, 0.2M$, the critical shadow radius calculated using expression (30) is not continuous when black hole charge reaches a critical value $Q = Q_{\text{discontinuity}}$. This is caused by the discontinuity of unstable photon sphere positions in the vicinity of Euler-Heisenberg black hole. When black hole charge excesses this critical value, the number of unstable photon sphere around Euler-Heisenberg black hole undergoes a sudden change³. Once the black hole charge comes across the discontinuity point (namely $Q > Q_{\text{discontinuity}}$), it is questionable that the results obtained using expression (30) could still represent a conventional “black hole shadow” or not. This issue deserves a more deeply study in the future.

5 Conclusions

In this work, the gravitational lensing of Euler-Heisenberg black hole surrounded by PFDM is studied. This kind of black hole solution, which are solved from the gravitational field equation coupled with nonlinear electromagnetic field and dark matter field, could give rise to the nonlinear electrodynamics effects and PFDM effects in charge black hole systems. It provide us a simply way to investigate the interplay of nonlinear electrodynamics effects (or QED effects) and dark matter effects on the studies of black holes. These effects coming from nonlinear electrodynamics and dark matter can be parameterized by parameters a and λ_{DM} respectively. In the presented work, we mainly focus on the gravitational lensing observables for Euler-Heisenberg black hole surrounded by PFDM. The gravitational deflection angle of light, time delay of light, precession angle and trajectories of massive object’s bound orbits, black hole shadow are calculated numerically from geodesics.

Our numerical results presented in this work show that influences coming from black hole electric charge, nonlinear electromagnetic effects, dark matter effects exhibit a similar tend for various gravitational lensing observables (including the gravitational deflection angle of light, time delay of light, precession angle of massive object’s bound orbits, and the black hole shadow size). Firstly, the Euler-Heisenberg black hole

³When black hole charge satisfies $Q < Q_{\text{discontinuity}}$, there are two unstable photon spheres near the Euler-Heisenberg black hole (surrounded by PFDM), and the outer branch of unstable photon sphere determines the black hole shadow size via expression (30). When black hole charge becomes $Q > Q_{\text{discontinuity}}$, there is only one unstable photon sphere. The outer branch of unstable photon spheres in the $Q < Q_{\text{discontinuity}}$ cases is disappeared, which makes the unstable photon sphere position undergo a sudden change when black hole charge come across the critical point $Q = Q_{\text{discontinuity}}$.

surround by PFDM with a larger electric charge could reduce the gravitational deflection angle, time delay of light, precession angle of bound orbits and black hole shadow radius. Secondly, the nonlinear electrodynamics effects parameterized by a has very tiny influences on these gravitational lensing observables. Thirdly, the most significant impacts on these gravitational lensing observables coming from the dark matter effects. The gravitational deflection angle, time delay of light, precession angle of bound orbits and black hole shadow radius are all greatly changed when PFDM parameter λ_{DM} is varied. Particularly, a larger PFDM parameter could greatly reduce the gravitational deflection angle, time delay of light and precession angle of bound orbits. This can be explained from the spacetime metric function (6) for Euler-Heisenberg black hole surrounded by PFDM, in which the PFDM parameter plays a role of “effective mass”. A positive PFDM parameter contributes to a negative “effective mass” in the spacetime metric, therefore it can diminish the gravitational lensing observables. Moreover, the dark matter also has notable influences on the shape and eccentricity of massive object’s bound orbits. For black hole shadow size, when PFDM parameter is smaller than a critical value, the black hole shadow radius reduced as the increasing of PFDM parameter. When PFDM parameter exceeds this critical value, the black hole shadow radius could be magnified when PFDM parameter increases. The critical value of PFDM parameter is roughly $0.5M < \lambda_{\text{critical}} < 0.8M$ for different black hole charge values.

We hope that the results in our present work can deepen our understanding of the nonlinear electrodynamics effects / QED effects and dark matter effects on the gravitational lensing of charged black hole systems. Hopefully it may have potential applications for theoretical and observational probing for dark matter effects in black holes and gravitation. Since the dark matter could significantly influence the gravitational lensing observables, the PFDM parameter can be constrained from gravitational lensing observations, by analyzing and comparing the observed data with theoretical predictions, especially with the help of accumulating observational data for supermassive black hole in galaxy centers. However, the nonlinear electrodynamics effects have very tiny influences on these gravitational lensing observables, so it would be not easy to probe the nonlinear electrodynamics in gravitational lensing observations (unless very high-precision observational data are employed).

Acknowledgment

The authors thanks Song-Lin Lyu and Guang-Zhou Guo for helpful discussion and comments on the numerical schemes. This research was funded by the Natural Science Foundation of Chongqing Municipality (Grant No. CSTB2022NSCQ-MSX0932), the Scientific and Technological Research Program of Chongqing Municipal Education Commission (Grant No. KJQN202201126 and No. KJQN202301164), the Scientific Research Program of Chongqing Science and Technology Commission (the Chongqing “zhitongche” program for doctors, Grant No. CSTB2022BSXM-JCX0100), the Scientific Research Foundation of Chongqing University of Technology (Grant No. 2020ZDZ027) and the Research and Innovation Team Cultivation Program of Chongqing University of Technology (Grant No. 2023TDZ007).

A Horizons for Euler-Heisenberg Black Hole Surrounded by Perfect Fluid Dark Matter

This appendix presents results on horizons for Euler-Heisenberg black hole surrounded by PFDM. The radii of horizons can be solved from the metric component function

$$f(r_H) = 1 - \frac{2M}{r_H} + \frac{Q^2}{r_H^2} - \frac{aQ^4}{20r_H^6} + \frac{\lambda_{\text{DM}}}{r_H} \cdot \ln \frac{r_H}{|\lambda_{\text{DM}}|} = 0 \quad (31)$$

In the absence of nonlinear electrodynamics effects / QED effects and dark matter effects (with $a = 0$ and $\lambda_{\text{DM}} = 0$), the spacetime reduce to a conventional RN spacetime, resulting in two horizons for $Q < M$, a single horizon for extreme case $Q = M$, and a naked singularity at the center for $Q > M$. However, in the presence of nonlinear electrodynamics effects and dark matter effects, the horizon structure can be strongly influenced. In figure 8, we plot the horizon radius for Euler-Heisenberg black hole surrounded by PFDM, which are calculated by numerically solving equation (31).

From the upper left panel of figure 8, in the absence of nonlinear electrodynamics effects (with $a = 0$), it can be observed that dark matter does not have obvious influences on the structure of horizons. Without the nonlinear electrodynamics effects, charged black hole surrounded by PFDM still possesses two horizons

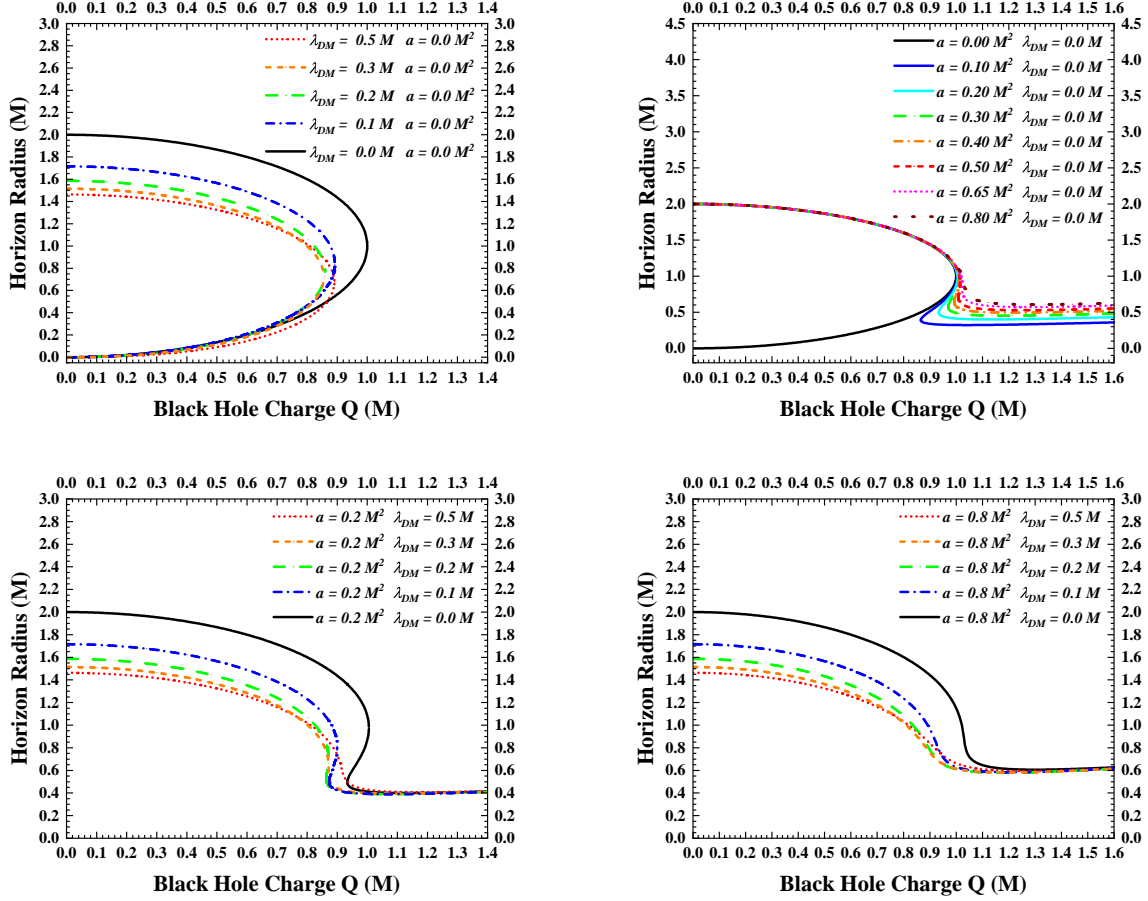


Figure 8: The horizons of Euler-Heisenberg black hole surrounded by PFDM. The multiple panels highlight the influences coming from dark matter effects and nonlinear electrodynamics effects. (a) The upper left panel shows the charged black hole's horizons affected by PFDM parameter λ_{DM} without the nonlinear electrodynamics effects (with $a = 0$). (b) The upper right panel shows the Euler-Heisenberg black hole's horizons affected by nonlinear electrodynamics effects (parameterized by a) without PFDM. (c) The lower left panel plots the horizon radius of Euler-Heisenberg black hole in the presence of dark matter and nonlinear electrodynamics (with $a = 0.2 M^2$). (d) The lower right panel plots the horizon radius of Euler-Heisenberg black hole in the presence of dark matter and nonlinear electrodynamics (with $a = 0.8 M^2$). In all four panels of this figure, the horizon radius, black hole electric charge Q , PFDM parameter λ_{DM} and nonlinear electrodynamics parameter a are given in unit of black hole mass M .

(inner and outer horizons) when $0 < Q < Q_{\text{extreme}}$. When the black hole charge exceeds the extremal black hole charge ($Q > Q_{\text{extreme}}$), the spacetime becomes horizon-less and produces a naked singularity in the center $r = 0$. In the presence of PFDM, the extremal black hole charge Q_{extreme} become decreased than the conventional RN case. This can be explained from the “effective mass” role that PFDM played in spacetime metric (6), as we have explained in section 4. A positive PFDM parameter contributes to a negative “effective mass” in spacetime metric, thus the corresponding extremal black hole charge is less than black hole mass ($Q_{\text{extreme}} < M$) for a given positive PFDM parameter ($\lambda_{\text{DM}} > 0$).

In the presence nonlinear electrodynamics effects (with $a > 0$), the horizon structure for charged Euler-Heisenberg black holes can be dramatically changed, which are clearly shown in the upper right panel of figure 8. Firstly, the naked singularity no longer exists when nonlinear electrodynamics is included ($a > 0$). For any given black hole charge, there is at least one horizon in Euler-Heisenberg black hole. Secondly, for a small black hole charge, the Euler-Heisenberg black hole has only one horizon, unlike the two horizon behavior (the inner and outer horizons) for pure RN spacetime with $a = 0$. In the upper right panel of figure 8, various curves correspond to positive nonlinear electrodynamics parameter values ($a > 0$) in the branch $M < r_H < 2M$ and $Q < M$ are almost overlapped with each other, but only the pure RN black hole with $a = 0$ has a second branch at $0 < r_H < M$ and $Q < M$ (labeled by black solid curve in the upper right panel). Thirdly, if the black hole electric charge fall into region $0.85M < Q < 1.02M$, the Euler-Heisenberg black hole with a small nonlinear electrodynamics parameter ($a < 0.5M^2$) could have three horizons. However, a larger nonlinear electrodynamics parameter (for instance the $a = 0.65M^2$ and $a = 0.8M^2$ in the upper right panel of figure 8) could prevent the occurrence of three horizons in Euler-Heisenberg black hole, producing a single horizon for arbitrary electric charge values.

When taking into account both nonlinear electrodynamics effects (with $a > 0$) and dark matter effects (with $\lambda_{\text{DM}} > 0$), the horizons of Euler-Heisenberg black hole surrounded by PFDM are plotted in the lower panels of figure 8, for nonlinear electrodynamics parameters $a = 0.2M^2$ and $a = 0.8M^2$ respectively. Comparing the positions of horizon for Euler-Heisenberg black hole without dark matter (in the upper right panel) and those in the presence of dark matter (in the lower left and lower right panels), we can obtain the following conclusions. In the presence of dark matter and nonlinear electrodynamics, the naked singularity is no longer emerged for arbitrary black hole electric charge, which is the same as that for Euler-Heisenberg black hole without PFDM. The dark matter influences the horizon size and changes the wide of three horizon region in the parameter space of black hole charge. A positive PFDM parameter ($\lambda_{\text{DM}} > 0$) results in smaller horizon radius, which can be explained using the “effective mass” role the PFDM played in spacetime metric. Furthermore, a positive PFDM parameter narrows the three horizon region in the parameter space of black hole charge. For instance, when nonlinear electrodynamics parameter gets value $a = 0.2M^2$, the three horizon region get narrowed for $0 < \lambda_{\text{DM}} \leq 0.3M$ (compared with those without PFDM plotted in the upper right panel), while the $\lambda_{\text{DM}} = 0.5M$ case does not possess a three horizon region. For a large nonlinear electrodynamics parameter (such as $a = 0.8M^2$ in the lower right panel), the Euler-Heisenberg black hole in the presence of dark matter does not possess a three horizons region, no matter what the PFDM parameter is varied.

References

- [1] P. A. R. Ade *et al.* (Planck Collaboration), Planck 2013 results. I. Overview of products and scientific results, *Astron. Astrophys.* **2014**, 571, A1. arXiv:1303.5062[astro-ph.CO]
- [2] P. A. R. Ade *et al.* (Planck Collaboration), Planck 2013 results. XVI. Cosmological parameters, *Astron. Astrophys.* **2014**, 571, A16.
- [3] N. Aghanim *et al.* (Planck Collaboration), Planck 2018 results. I. Overview and the cosmological legacy of Planck, *Astron. Astrophys.* **2020**, 641, A1. arXiv:1807.06205[astro-ph.CO]
- [4] N. Aghanim *et al.* (Planck Collaboration), Planck 2018 results. VI. Cosmological parameters, *Astron. Astrophys.* **2020**, 641, A6. Erratum: *Astron. Astrophys.* **2021**, 652, C4. arXiv:1807.06209[astro-ph.CO]
- [5] V. C. Rubin and W. K. Ford, Jr., Rotation of the Andromeda Nebula from a Spectroscopic Survey of Emission Regions, *Astrophys. J.* **1970**, 159, 379-403.
- [6] Y. Sofue and V. Rubin, Rotation curves of spiral galaxies, *Ann. Rev. Astron. Astrophys.* **2001**, 39, 137-174. arXiv:astro-ph/0010594[astro-ph]
- [7] E. Corbelli and P. Salucci, The Extended Rotation Curve and the Dark Matter Halo of M33, *Mon. Not. Roy. Astron. Soc.* **2000**, 311, 441-447. arXiv:astro-ph/9909252[astro-ph]

- [8] G. Bertone and D. Hooper, History of dark matter, *Rev. Mod. Phys.* **2018**, 90, 045002. arXiv:1605.04909[astro-ph.CO]
- [9] Z. Xu, X. Hou, X. Gong and J. Wang, Black Hole Space-time In Dark Matter Halo, *J. Cosmol. Astropart. Phys.* **2018**, 09, 038. arXiv:1803.00767[gr-qc]
- [10] X. Hou, Z. Xu, M. Zhou and J. Wang, Black hole shadow of Sgr A* in dark matter halo, *J. Cosmol. Astropart. Phys.* **2018**, 07, 015. arXiv:1804.08110[gr-qc]
- [11] K. Jusufi, M. Jamil, P. Salucci, T. Zhu and S. Haroon, Black Hole Surrounded by a Dark Matter Halo in the M87 Galactic Center and its Identification with Shadow Images, *Phys. Rev. D* **2019**, 100, 044012. arXiv:1905.11803[physics.gen-ph]
- [12] K. Jusufi, Quasinormal Modes of Black Holes Surrounded by Dark Matter and Their Connection with the Shadow Radius, *Phys. Rev. D* **2020**, 101, 084055.
- [13] K. Jusufi, M. Jamil and T. Zhu, Shadows of Sgr A* black hole surrounded by superfluid dark matter halo, *Eur. Phys. J. C* **2020**, 80, 354.
- [14] S. Nampalliwar, S. Kumar, K. Jusufi, Q. Wu, M. Jamil and P. Salucci, Modeling the Sgr A* Black Hole Immersed in a Dark Matter Spike, *Astrophys. J.* **2021**, 916, 116. arXiv:2103.12439[astro-ph.HE]
- [15] R. C. Pantig, P. K. Yu, E. T. Rodulfo and A. Övgün, Shadow and weak deflection angle of extended uncertainty principle black hole surrounded with dark matter, *Annals Phys.* **2022**, 436, 168722. arXiv:2104.04304[gr-qc]
- [16] R. C. Pantig and A. Övgün, Dark matter effect on the weak deflection angle by black holes at the center of Milky Way and M87 galaxies, *Eur. Phys. J. C* **2022**, 82, 391. arXiv:2201.03365[gr-qc]
- [17] R. C. Pantig and A. Övgün, Dehnen halo effect on a black hole in an ultra-faint dwarf galaxy, *J. Cosmol. Astropart. Phys.* **2022**, 08, 056. arXiv:2202.07404[astro-ph.GA]
- [18] R. C. Pantig and A. Övgün, Black Hole in Quantum Wave Dark Matter, *Fortsch. Phys.* **2023**, 71, 2200164. arXiv:2210.00523[gr-qc]
- [19] R. A. Konoplya and A. Zhidenko, Solutions of the Einstein Equations for a Black Hole Surrounded by a Galactic Halo, *Astrophys. J.* **2022**, 933, 166. arXiv:2202.02205[gr-qc]
- [20] S. V. M. C. B. Xavier, H. C. D. Lima, Junior. and L. C. B. Crispino, Shadows of black holes with dark matter halo, *Phys. Rev. D* **2023**, 107, 064040. arXiv:2303.17666[gr-qc]
- [21] Y. Yang, D. Liu, A. Övgün, G. Lambiase and Z. W. Long, Black hole surrounded by the pseudo-isothermal dark matter halo, *Eur. Phys. J. C* **2024**, 84, 63. arXiv:2308.05544[gr-qc]
- [22] D. Liu, Y. Yang, A. Övgün, Z. W. Long and Z. Xu, Gravitational ringing and superradiant instabilities of the Kerr-like black holes in a dark matter halo, *Eur. Phys. J. C* **2023**, 83, 565. arXiv:2204.11563[gr-qc]
- [23] D. Liu, Y. Yang, Z. Xu and Z. W. Long, Modeling the black holes surrounded by a dark matter halo in the galactic center of M87, *Eur. Phys. J. C* **2024**, 84, 136. arXiv:2307.13553[gr-qc]
- [24] Y. G. Liu, C. K. Qiao and J. Tao, Gravitational Lensing of Spherically Symmetric Black Holes in Dark Matter Halos, *J. Cosmol. Astropart. Phys.* **2024**, 10, 075. arXiv:2312.15760[gr-qc]
- [25] C. K. Qiao and P. Su, Time Delay of Light in the Gravitational lensing of Supermassive Black Holes in Dark Matter Halos, *Eur. Phys. J. C* **2024**, 84, 1032. arXiv:2403.05682[gr-qc]
- [26] R. C. Pantig, Apparent and emergent dark matter around a Schwarzschild black hole, *Phys. Dark Univ.* **2024**, 45, 101550. arXiv:2405.07531[gr-qc]
- [27] F. Rahaman, K. K. Nandi, A. Bhadra, M. Kalam and K. Chakraborty, Perfect Fluid Dark Matter, *Phys. Lett. B* **2011**, 694, 10-15. arXiv:1009.3572[gr-qc]
- [28] J. Barranco, A. Bernal and D. Nunez, Dark matter equation of state from rotational curves of galaxies, *Mon. Not. Roy. Astron. Soc.* **2015**, 449, 403-413. arXiv:1301.6785[astro-ph.CO]
- [29] A. A. Potapov, G. M. Garipova and K. K. Nandi, Revisiting perfect fluid dark matter: Observational constraints from our galaxy, *Phys. Lett. B* **2016**, 753, 140-146. arXiv:1606.07733[gr-qc]
- [30] V. V. Kiselev, Quintessence and black holes, *Class. Quant. Grav.* **2003**, 20, 1187-1198. arXiv:gr-qc/0210040
- [31] V. V. Kiselev, Quintessential solution of dark matter rotation curves and its simulation by extra dimensions, arXiv:gr-qc/0303031.
- [32] M. H. Li, K. C. Yang, Galactic dark matter in the phantom field, *Phys. Rev. D* **2012**, 86, 123015. arXiv:1204.3178[astro-ph.CO]
- [33] Y. Heydarzade and F. Darabi, Black Hole Solutions Surrounded by Perfect Fluid in Rastall Theory, *Phys. Lett. B* **2017**, 771, 365-373 (2017) arXiv:1702.07766 [gr-qc]

- [34] A. Das, A. Saha and S. Gangopadhyay, Investigation of circular geodesics in a rotating charged black hole in the presence of perfect fluid dark matter, *Class. Quant. Grav.* **2021**, 28, 065015. arXiv:2009.03644[gr-qc]
- [35] Z. Xu, J. Wang and X. Hou, Kerr–anti-de Sitter/de Sitter black hole in perfect fluid dark matter background, *Class. Quant. Grav.* **2018**, 35, 115003. arXiv:1711.04538[gr-qc]
- [36] Z. Xu, X. Hou, X. Gong and J. Wang, Kerr–Newman-AdS black hole surrounded by perfect fluid matter in Rastall gravity, *Eur. Phys. J. C* **2018**, 78, 513. arXiv:1711.04542[gr-qc]
- [37] M. Rizwan, M. Jamil and K. Jusufi, Distinguishing a Kerr-like black hole and a naked singularity in perfect fluid dark matter via precession frequencies, *Phys. Rev. D* **2019**, 99, 024050. arXiv:1812.01331[gr-qc]
- [38] S. Haroon, M. Jamil, K. Jusufi, K. Lin and R. B. Mann, Shadow and Deflection Angle of Rotating Black Holes in Perfect Fluid Dark Matter with a Cosmological Constant, *Phys. Rev. D* **2019**, 99, 044015. arXiv:1810.04103[gr-qc]
- [39] X. Hou, Z. Xu and J. Wang, Rotating Black Hole Shadow in Perfect Fluid Dark Matter, *J. Cosmol. Astropart. Phys.* **2018**, 12, 040. arXiv:1810.06381[gr-qc]
- [40] Z. Xu, X. Hou, J. Wang and Y. Liao, Perfect fluid dark matter influence on thermodynamics and phase transition for a Reissner-Nordstrom-anti-de Sitter black hole, *Adv. High Energy Phys.* **2019**, 2019, 2434390. arXiv:1610.05454[gr-qc]
- [41] B. Narzilloev, J. Rayimbaev, S. Shaymatov, A. Abdujabbarov, B. Ahmedov and C. Bambi, Dynamics of test particles around a Bardeen black hole surrounded by perfect fluid dark matter, *Phys. Rev. D* **2020**, 102, 104062. arXiv:2011.06148[gr-qc]
- [42] F. Atamurotov, A. Abdujabbarov and W. B. Han, Effect of plasma on gravitational lensing by a Schwarzschild black hole immersed in perfect fluid dark matter, *Phys. Rev. D* **2021**, 104, 084015.
- [43] Y. Cao, H. Feng, W. Hong and J. Tao, Joule-Thomson expansion of RN-AdS black hole immersed in perfect fluid dark matter, *Commun. Theor. Phys.* **2021**, 73, 095403. arXiv:2101.08199[gr-qc]
- [44] X. Zhou, Y. Xue, B. Mu and J. Tao, Temporal and spatial chaos of RN-AdS black holes immersed in Perfect Fluid Dark Matter, *Phys. Dark Univ.* **2023**, 39, 101168. arXiv:2209.03612[gr-qc]
- [45] X. J. Gao, X. K. Yan, Y. Yin and Y. P. Hu, Gravitational lensing by a charged spherically symmetric black hole immersed in thin dark matter, *Eur. Phys. J. C* **2023**, 83, 281. arXiv:2303.00190[gr-qc]
- [46] M. Heydari-Fard, S. G. Honarvar and M. Heydari-Fard, Thin accretion disc luminosity and its image around rotating black holes in perfect fluid dark matter, *Mon. Not. Roy. Astron. Soc.* **2023**, 521, 708-716. arXiv:2210.04173[gr-qc]
- [47] G. Abbas and R. H. Ali, Thermal fluctuations, quasi-normal modes and phase transition of the charged AdS black hole with perfect fluid dark matter, *Eur. Phys. J. C* **2023**, 83, 407. arXiv:2305.05541[gr-qc]
- [48] C. K. Qiao and M. Zhou, Gravitational lensing of Schwarzschild and charged black holes immersed in perfect fluid dark matter halo, *J. Cosmol. Astropart. Phys.* **2023**, 2023(12), 005. arXiv:2212.13311[gr-qc]
- [49] A. Das, A. Saha and S. Gangopadhyay, Study of circular geodesics and shadow of rotating charged black hole surrounded by perfect fluid dark matter immersed in plasma, *Class. Quant. Grav.* **2022**, 39, 075005. arXiv:2110.11704[gr-qc]
- [50] A. Das, A. R. Chowdhury and S. Gangopadhyay, Stability, quasinormal modes in a charged black hole in perfect fluid dark matter, *Class. Quant. Grav.* **2024**, 41, 015018. arXiv:2306.00646[gr-qc]
- [51] X. Yang, Observational appearance of the spherically symmetric black hole in PFDM, *Phys. Dark Univ.* **2024**, 44, 101467.
- [52] H. Yajima and T. Tamaki, Black hole solutions in Euler-Heisenberg theory, *Phys. Rev. D* **2001**, 63, 064007. arXiv:gr-qc/0005016[gr-qc]
- [53] S. I. Kruglov, Remarks on Heisenberg-Euler-type electrodynamics, *Mod. Phys. Lett. A* **2017**, 32, 1750092. arXiv:1705.08745[physics.gen-ph]
- [54] N. Bretón, C. Lämmerzahl and A. Macías, Rotating black holes in the Einstein-Euler-Heisenberg theory, *Class. Quant. Grav.* **2019**, 36, 235022.
- [55] G. G. L. Nashed and S. Nojiri, Mimetic Euler-Heisenberg theory, charged solutions, and multihorizon black holes, *Phys. Rev. D* **2021**, 104, 044043. arXiv:2107.13550[gr-qc]
- [56] W. Heisenberg and H. Euler, Consequences of Dirac Theory of the Positron, *Z. Phys.* **1936**, 98, 714-732.
- [57] N. Breton and L. A. Lopez, Quasinormal modes of nonlinear electromagnetic black holes from unstable null geodesics, *Phys. Rev. D* **2016**, 94, 104008. arXiv:1607.02476[gr-qc]

- [58] L. Gulin and I. Smolić, Generalizations of the Smarr formula for black holes with nonlinear electromagnetic fields, *Class. Quant. Grav.* **2018**, 35, 025015. arXiv:1710.04660[gr-qc]
- [59] A. Allahyari, M. Khodadi, S. Vagnozzi and D. F. Mota, Magnetically charged black holes from nonlinear electrodynamics and the Event Horizon Telescope, *J. Cosmol. Astropart. Phys.* **2020**, 2020, 003. arXiv:1912.08231[gr-qc]
- [60] D. Magos and N. Bretón, Thermodynamics of the Euler-Heisenberg-AdS black hole, *Phys. Rev. D* **2020**, 102, 084011. arXiv:2009.05904[gr-qc]
- [61] J. C. Olvera and L. A. López, Scattering and absorption sections of nonlinear electromagnetic black holes, *Eur. Phys. J. Plus* **2020**, 135, 288. arXiv:1910.03067[gr-qc]
- [62] D. Amaro and A. Macías, Geodesic structure of the Euler-Heisenberg static black hole, *Phys. Rev. D* **102**, 102, 104054.
- [63] M. Maceda, A. Macias and D. Martinez-Carbajal, Shadow of a noncommutative-inspired Einstein-Euler-Heisenberg black hole, *Int. J. Mod. Phys. A* **2021**, 36, 2150191. arXiv:2008.07040[gr-qc]
- [64] Z. Hu, Z. Zhong, P. C. Li, M. Guo and B. Chen, QED effect on a black hole shadow, *Phys. Rev. D* **2021**, 103, 044057. arXiv:2012.07022[gr-qc]
- [65] Z. Zhong, Z. Hu, H. Yan, M. Guo and B. Chen, QED effects on Kerr black hole shadows immersed in uniform magnetic fields, *Phys. Rev. D* **2021**, 104, 104028. arXiv:2108.06140[gr-qc]
- [66] Q.-M. Fu, L. Zhao and Y.-X. Liu, Weak deflection angle by electrically and magnetically charged black holes from nonlinear electrodynamics, *Phys. Rev. D* **2021**, 104, 024033. arXiv:2101.08409[gr-qc]
- [67] X. J. Gao, J. M. Chen, H. Zhang, Y. Yin and Y. P. Hu, Investigating strong gravitational lensing with black hole metrics modified with an additional term, *Phys. Lett. B* **2021**, 822, 136683. arXiv:2108.09409[gr-qc]
- [68] N. Bretón and L. A. López, Birefringence and quasinormal modes of the Einstein-Euler-Heisenberg black hole, *Phys. Rev. D* **2021**, 104, 024064. arXiv:2105.12283[gr-qc]
- [69] D. Amaro and A. Macías, Exact lens equation for the Einstein-Euler-Heisenberg static black hole, *Phys. Rev. D* **2022**, 106, 064010.
- [70] Y. Kumaran and A. Övgün, Deflection Angle and Shadow of the Reissner-Nordström Black Hole with Higher-Order Magnetic Correction in Einstein-Nonlinear-Maxwell Fields, *Symmetry* **2022**, 14, 2054. arXiv:2210.00468[gr-qc]
- [71] W. Javed, M. Atique and A. Övgün, Effects of electric and magnetic charges on weak deflection angle and bounding greybody of black holes in nonlinear electrodynamics, *New Astron.* **2023**, 104, 102064.
- [72] K. Nomura and D. Yoshida, Quasinormal modes of charged black holes with corrections from nonlinear electrodynamics, *Phys. Rev. D* **2022**, 105, 044006. arXiv:2111.06273[gr-qc]
- [73] X. X. Zeng, K. J. He, G. P. Li, E. W. Liang and S. Guo, QED and accretion flow models effect on optical appearance of Euler–Heisenberg black holes, *Eur. Phys. J. C* **2022**, 82, 764.. arXiv:2209.05938[gr-qc]
- [74] Z. Luo and J. Li, Gravitational perturbations of the Einstein-Euler-Heisenberg black hole, *Chin. Phys. C* **2022**, 46, 085107.
- [75] X. Ye, Z. Q. Chen, M. D. Li and S. W. Wei, QED effects on phase transition and Ruppeiner geometry of Euler-Heisenberg-AdS black holes, *Chin. Phys. C* **2022**, 46, 115102. arXiv:2202.09053[gr-qc]
- [76] H. Dai, Z. Zhao and S. Zhang, Thermodynamic phase transition of Euler-Heisenberg-AdS black hole on free energy landscape, *Nucl. Phys. B* **2023**, 991, 116219. arXiv:2202.14007[gr-qc]
- [77] G. R. Li, S. Guo and E. W. Liang, High-order QED correction impacts on phase transition of the Euler-Heisenberg AdS black hole, *Phys. Rev. D* **2022**, 106, 064011. arXiv:2111.10812[hep-th]
- [78] D. Chen and C. Gao, Angular momentum and chaos bound of charged particles around Einstein–Euler–Heisenberg AdS black holes, *New J. Phys.* **2022**, 24, 123014. arXiv:2205.08337[hep-th]
- [79] B. Q. Wang and S. R. Wu, Thermodynamic properties of the Euler-Heisenberg-AdS black hole under new higher order generalized uncertainty principle, *Indian J. Phys.* **2023**, 97, 3133-3141.
- [80] Q. Yu, Q. Xu and J. Tao, Thermodynamics and microstructures of Euler–Heisenberg black hole in a cavity, *Commun. Theor. Phys.* **2023**, 75, 095402. arXiv:2302.09821[gr-qc]
- [81] N. Bretón, C. Lämmerzahl and A. Macías, Rotating structure of the Euler-Heisenberg black hole, *Phys. Rev. D* **2022**, 105, 104046.
- [82] H. Rehman, G. Abbas, T. Zhu and G. Mustafa, Matter accretion onto the magnetically charged Euler-Heisenberg black hole with scalar hair, *Eur. Phys. J. C* **2023**, 83, 856. arXiv:2307.16155[gr-qc]
- [83] M. R. Alipour, M. A. S. Afshar, S. Noori Gashti and J. Sadeghi, Topological classification and black hole thermodynamics, *Phys. Dark Univ.* **2023**, 42, 101361. arXiv:2305.05595[gr-qc]

- [84] A. R. Soares, R. L. L. Vitória and C. F. S. Pereira, Gravitational lensing in a topologically charged Eddington-inspired Born–Infeld spacetime, *Eur. Phys. J. C* **2023**, 83, 903. arXiv:2305.11105[gr-qc]
- [85] N. J. Gogoi and P. Phukon, Thermodynamic topology of 4D Euler–Heisenberg–AdS black hole in different ensembles, *Phys. Dark Univ.* **2024**, 44, 101456. arXiv:2312.13577[hep-th]
- [86] D. P. Theodosopoulos, T. Karakasis, G. Koutsoumbas and E. Papantonopoulos, Motion of particles around a magnetically charged Euler–Heisenberg black hole with scalar hair and the Event Horizon Telescope, *Eur. Phys. J. C* **2024**, 84, 592. arXiv:2311.02740[gr-qc]
- [87] S. V. Bolokhov, Late time decay of scalar and Dirac fields around an asymptotically de Sitter black hole in the Euler–Heisenberg electrodynamics, *Eur. Phys. J. C* **2024**, 84, 634. arXiv:2404.09364[gr-qc]
- [88] R. H. Ali, G. Abbas and G. Mustafa, Effect of scalar hair on magnetically charge Euler-Heisenberg AdS black hole via extended phase transition, *Phys. Dark Univ.* **2024**, 44, 101465.
- [89] G. Lambiase, D. J. Gogoi, R. C. Pantig and A. Övgün, Shadow and quasinormal modes of the rotating Einstein-Euler-Heisenberg black holes, arXiv:2406.18300[gr-qc].
- [90] Y. Sekhmani, S. N. Gashti, M. A. S. Afshar, M. R. Alipour, J. Sadeghi, J. Rayimbaev, Thermodynamic topology of Black Holes in $F(R)$ -Euler-Heisenberg gravity’s Rainbow, arXiv:2409.04997[gr-qc].
- [91] S. J. Ma, R. B. Wang, J. B. Deng and X. R. Hu, Euler-Heisenberg black hole surrounded by perfect fluid dark matter. *Eur. Phys. J. C* **2024**, 84, 595. arXiv:2401.03187[gr-qc]
- [92] G. D. A. Yildiz, A. Ditta, A. Ashraf, E. Güdekli, Y. M. Alanazi and A. Reyimberganov, Optical properties of Euler–Heisenberg black hole surrounded by perfect fluid dark matter. *Phys. Dark Univ.* **2024**, 46, 101583.
- [93] L. You, R. B. Wang, S. J. Ma, J. B. Deng and X. R. Hu, Optical properties of Euler-Heisenberg black hole in the Cold Dark Matter Halo. arXiv:2403.12840[gr-qc].
- [94] B. Hamil and B. C. Lütüoğlu, Euler-Heisenberg black hole surrounded by quintessence in the background of perfect fluid dark matter: Thermodynamics, Shadows and Quasinormal modes, arXiv:2406.02109[gr-qc]
- [95] S. Mollerach and E. Roulet, *Gravitational Lensing and Microlensing*, World Scientific: Singapore, 2002; pp. 1-191. doi:10.1142/4890
- [96] A. Chowdhuri, S. Ghosh and A. Bhattacharyya, A review on analytical studies in Gravitational Lensing, *Front. Phys.* **2023**, 11, 1113909. arXiv:2303.02069[gr-qc]
- [97] K. Akiyama *et al.* [Event Horizon Telescope], First M87 Event Horizon Telescope Results. I. The Shadow of the Supermassive Black Hole, *Astrophys. J. Lett.* **2019**, 875, L1. arXiv:1906.11238[astro-ph.GA]
- [98] K. Akiyama *et al.* [Event Horizon Telescope], First M87 Event Horizon Telescope Results. IV. Imaging the Central Supermassive Black Hole, *Astrophys. J. Lett.* **2019**, 875, L4. arXiv:1906.11241[astro-ph.GA]
- [99] K. Akiyama *et al.* [Event Horizon Telescope], First Sagittarius A* Event Horizon Telescope Results. I. The Shadow of the Supermassive Black Hole in the Center of the Milky Way, *Astrophys. J. Lett.* **2022**, 930, L12. arXiv:2311.08680[astro-ph.HE]
- [100] V. Cardoso, K. Destounis, F. Duque, R. P. Macedo and A. Maselli, Black holes in galaxies: Environmental impact on gravitational-wave generation and propagation, *Phys. Rev. D* **2022**, 105, L061501. arXiv:2109.00005[gr-qc]
- [101] R. A. Konoplya and A. Zhidenko, Solutions of the Einstein Equations for a Black Hole Surrounded by a Galactic Halo,” *Astrophys. J.* **2022**, 933, 166. arXiv:2202.02205[gr-qc]
- [102] A. Övgün and R. C. Pantig, Black hole in the Dekel-Zhao dark matter profile, arXiv:2501.12559[gr-qc].
- [103] R. G. Daghigh and G. Kunstatter, Effect of dark matter on galactic black hole ringdown waveforms and shadows, *Phys. Rev. D* **2024**, 109, 083004. arXiv:2308.15682[gr-qc]
- [104] D. Liu, Black holes surrounded by dark matter spike: spacetime metrics and gravitational wave ringdown waveforms, arXiv:2501.12213[gr-qc].
- [105] A. Ishihara, Y. Suzuki, T. Ono, T. Kitamura, and H. Asada, Gravitational bending angle of light for finite distance and the Gauss-Bonnet theorem, *Phys. Rev. D* **2016**, 94, 084015. arXiv:1604.08308[gr-qc]
- [106] A. Ishihara, Y. Suzuki, T. Ono and H. Asada, Finite-distance corrections to the gravitational bending angle of light in the strong deflection limit, *Phys. Rev. D* **2017**, 95, 044017. arXiv:1612.04044[gr-qc]
- [107] T. Ono and H. Asada, The effects of finite distance on the gravitational deflection angle of light, *Universe* **2018**, 5, 218. arXiv:1906.02414[gr-qc]

- [108] K. Takizawa, T. Ono, and H. Asada, Gravitational deflection angle of light: Definition by an observer and its application to an asymptotically nonflat spacetime, *Phys. Rev. D* **2020**, 101, 104032. arXiv:2001.03290[gr-qc]
- [109] K. Takizawa, T. Ono and H. Asada, Gravitational lens without asymptotic flatness: Its application to the Weyl gravity, *Phys. Rev. D* **2020**, 102, 064060. arXiv:2006.00682[gr-qc]
- [110] C. K. Qiao and M. Li, Geometric approach to circular photon orbits and black hole shadows, *Phys. Rev. D* **2022**, 106, L021501. arXiv:2204.07297[gr-qc]
- [111] C. K. Qiao, Curvatures, photon spheres, and black hole shadows, *Phys. Rev. D* **2022**, 106, 084060. arXiv:2208.01771[gr-qc]
- [112] C. K. Qiao, The Existence and Distribution of Photon Spheres Near Spherically Symmetric Black Holes – A Geometric Analysis, arXiv:2407.14035[gr-qc].